T.R.
ONDOKUZ MAYIS UNIVERSITY
INSTITUTE OF GRADUATE STUDIES
DEPARTMENT OF NANOSCIENCE AND NANOTECHNOLOGY

METAL-ORGANIC FRAMEWORK COMPOSITE BASED MATERIALS FOR HYBRID SUPERCAPACITORS

Master's Thesis

Sarmad Hasan Ahmed AL-MAAWI

Supervisor

Prof. Dr. Ömer ANDAÇ

This thesis was supported by Ondokuz Mayıs University with project number PYO.FEN.1904.21.025

SAMSUN
2023

DECLARATION OF COMPLIANCE WITH SCIENTIFIC ETHIC

I hereby declare and undertake that I complied with scientific ethics and academic rules in all stages of my Master's Thesis , that I have referred to each quotation that I use directly or indirectly in the study and that the works I have used consist of those shown in the sources, that it was written in accordance with the institute writing guide and that the situations stated in the article 3, section 9 of the Regulation for TÜBİTAK Research and Publication Ethics Board were not violated.

Is Ethics Committee Necessary?

Yes ☐ (If it necessary, please add appendices.)

No ☒

05/01/ 2023

Sarmad Hasan Ahmed
AL-MAAWI

DECLARATION OF THE THESIS STUDY ORIGINALITY REPORT

Thesis Title : METAL-ORGANIC FRAMEWORK COMPOSITE BASED MATERIALS FOR HYBRID SUPERCAPACITORS

As a result of the originality report taken by me from the plagiarism detection program on 06 /01 /2023 for the thesis titled above;

Similarity ratio : % 20

Single resource rate : % 2 has been released.

05/01/ 2023

Prof. Dr. Ömer ANDAÇ

ÖZET

HİBRİT SÜPERKAPASİTÖRLER İÇİN METAL-ORGANİK KOMPOZİT TEMELLİ MALZEMELER

Sarmad Hasan Ahmed AL-MAAWI
Ondokuz Mayıs Üniversitesi
Lisansüstü Eğitim Enstitüsü
Nanobilim ve Nanoteknoloji Ana Bilim Dalı
Yüksek Lisans, Şubat/2023
Danışman: Prof. Dr. Ömer ANDAÇ

Pil benzeri ve kapasitif elektrotlardan oluşan hibrit süper kapasitörler, uygun güç ve yoğunlukları nedeniyle umut verici enerji depolama cihazları olarak kabul edilir. Yüksek özgül kapasitanslara, yüksek performansa ve istenen tokluğa sahip pil benzeri ve kapasitif elektrotların stili ve üretimi, hibrit süper kapasitörlerin genel enerji depolama performansını iyileştirmek için çok önemlidir. İşlevsel özelliklere, ayarlanabilir kimyasal yapılara sahip metal-organik yapılar (MOF), verimli hibrit süper kapasitörlerin yapımında kullanılabilir. Süper kapasitör uygulamalarında farklı tipte MOF kalsinasyonları incelenmiştir.

Bu çalışmada, metal öncülü olarak $Co(NO_3)_2.6H_2O$, organik ligantlar olarak 1,4-benzendikarboksilat(BDC) ve 1-vinilimidazol (1-VIM) kullanılarak standart solvotermal koşullar altında kobalt bazlı bir 2D koordinasyon polimeri hazırlandı. Çözücü olarak N,N-dimetilformamid (DMF) ve etanol kullanıldı.Solvotermal reaksiyonla 2D koordinasyon polimeri $[Co_3(BDC)_3(1\text{-}vim)_2]$ elde edildi ve termogravimetri/diferansiyel termal analiz (TA), toz X-ışını kırınımı (PXRD) ve Fourier dönüşümleri kızılötesi spektroskopisi (FTIR) ile karakterize edildi. TA sonuçları, $[Co_3(BDC)_3(1\text{-}vim)_2]$'nin üç ana aşamada ayrıştığını ve son olarak Co_3O_4 oluşumunun gözlendiğini doğruladı. FTIR sonuçlarında vinil, karboksil ve C—H'nin farklılaşması gözlendi. Oluşan kristal yapıları karakterize etmek için toz X-ışını verileri kullanıldı. Kobalt bazlı aktif maddeler olan Co_3O_4, ısıl işlemlerle elde edilmiş ve toz X-ışını kırınımı ile karakterize edilmiştir. Süper kapasitörler için elektrotların yapımında bağlayıcı malzeme olarak poliviniliden florür ve iletkenliği iyileştirmek için iletken karbon kullanıldı. $[Co_3(BDC)_3(1\text{-}vim)_2]$ ve Co_3O_4'ün elektrokimyasal performansı, KOH ve Na_2SO_4 elektrolitinde üç elektrotlu bir sistemde döngüsel voltammetri ve elektrokimyasal empedans spektroskopisi ile incelendi. Döngüsel voltametri sonuçlarının değerlendirilmesi için alan hesaplamaları yapıldı ve kapasite değerleri hesaplandı. Hesaplanan kapasite değerleri literatür ile karşılaştırmalı olarak verildi. Sonuçlar literatür değerleri ile uyumludur.

Anahtar Sözcükler: Süper kapasitörler, Metal-organik çerçeveler, 1, 4-Benzendikarboksilat, 1-Vinilimidazol, Koordinasyon polimeri

ABSTRACT

METAL-ORGANIC FRAMEWORK COMPOSITE BASED MATERIALS FOR HYBRID SUPERCAPACITORS

Sarmad Hasan Ahmed AL-MAAWI
Ondokuz Mayıs University
Institute of Graduate Studies
Department of Nanoscience and Nanotechnology
Master, February/2023
Supervisor: Prof. Dr. Ömer ANDAÇ

Hybrid supercapacitors, consisting of battery-like and capacitive electrodes, are considered promising energy storage devices due to their favorable power and density. The style and manufacture of battery-like and capacitive electrodes with high specific capacitances, high performance, and desired toughness are crucial to improving the overall energy storage performance of hybrid supercapacitors. Metal-organic frameworks (MOF) with functional properties, tunable chemical structures can result in preferable energy storage efficiencies of hybrid supercapacitors. Different types of MOF calcinations have been studied in supercapacitor applications

In this work, a cobalt-based 2D coordination polymer was prepared under standard solvothermal conditions using $Co(NO_3)_2.6H_2O$ as metal precursor, 1,4-benzenedicarboxylate(BDC) and 1-vinylimidazole (1-VIM) as organic ligants and N,N-dimethylformamide (DMF) and ethanol as solvents. 2D coordination polymer $[Co_3(BDC)_3(1\text{-}vim)_2]$ was obtained and chracterized by thermogravimetry/differential thermal analysis (TA), powder X-ray diffraction (PXRD) and Fourier transforms infrared spectroscopy (FTIR). TA results confirmed that $[Co_3(BDC)_3(1\text{-}vim)_2]$ decomposes in three main stages and the finally Co3O4 formation was observed. Vibration of vinily, carboxyl and C—H were observed in FTIR results. Powder X-ray data was used to characterise crystal structures formed. Cobalt-based active materials, Co_3O_4 was obtained by thermal treatments at diffrenet temperratures and chracterized by powder X-ray diffraction. Polyvinylidene fluoride was used as the binder material and and conductive carbon was used to improve the conductivity in making of electrodes for supercapacitors. Electrochemical performance of $[Co_3(BDC)_3(1\text{-}vim)_2]$ and Co_3O_4 were studied by the cyclic voltammetry in a three- electrode system in KOH and Na_2SO_4 electrolyte. The results are compatible with the literature values.

Keywords: Supercapacitors, Metal-organic frameworks, 1, 4-Benzenedicarboxylate, 1-Vinylimidazole, Coordination polymer.

ACKNOWLEDGEMENT

I would like to thank my advisor, Prof. Dr. To Ömer ANDAÇ,

To Faculty Members and Research Assistants of the Department of Chemistry;

To my dear family, who have shown all kinds of material and moral sacrifices and support throughout my education life,

I owe my deepest respect, love and thanks to.

Sarmad Hasan Ahmed AL-MAAWI

CONTENTS

SYMBOLS AND ABBREVIATIONS

BDC	: 1,4-Benzenedicarboxylate
DMF	: N,N-dimethylformamide
EDLC	: Electric double layer capacitor
FTIR:	:Fourier-transform infrared spectroscopy
MOF	: Metal-Organic Framework
SEM	: Scanning Electron Microscopy
1-VIM	: 1-Vinylimidazole

FIGURES LEGENDS

TABLES LEGENDS

1. INTRODUCTION

Climate change will significantly affect people's daily lives worldwide over the next 100 years. Environmental changes will lead to increased heat waves. Floods and wildfires will drive people from California, Florida, and the vulnerable Pacific Islands. Scientists believe global temperatures could rise by as much as 6 degrees Celsius by 2100, making many areas of the world permanently uninhabitable. Therefore, climate change is one of humanity's most significant changes this century.

On the other hand, Energy shortages and pollution are challenges people face in a population explosion and social development. By 2050, the world will demand twice as much energy as now. Today's worldwide supply of energy is highly depending on swiftly consumed, fossil fuels that aren't clean energy, like coal, natural gas, and oil & similar. At the same time, the high using fossil fuels is inevitable cause's emissions such as (CO_2, SO_2, and NOx, which are destructive to natural environment and people. In recent decades, the call for sustainable energy technologies has become louder and louder because of the never emitted pollutants and the high consumption of fossil fuels. Electric power, the much more prevalent form of energy use, may be created from renewable and environmentally friendly resources like solar, tidal or wind energy and offers excellent potential to sustainably meet our energy needs and change how people get around. Strategic projects such as electric vehicles (EVs) and hybrid electric vehicles have migrated from the drawers of academic labs to the desks of CEOs of industry giants worldwide. According to Forbes, global sales of electric cars have more than doubled since 2014. (D.-G. Wang, Liang, Gao, Qu, & Zou, 2020).

As the demand for electric and hybrid vehicles (EV/HEV) increases worldwide, the energy problem is becoming more serious. Supercapacitors can be developed with several advantages in response to the energy crisis. The supercapacitor is the best of both worlds regarding new energy storage devices. It has a low internal resistance, it indicates it has a high energy density, and can be recharged and discharged rapidly, and for long service life. Depending on the energy storage technique used, supercapacitors may be classified as electrical double-layer capacitors (ELDC) or (pseudocapacitors. Under the influence of an external force, the EDLC, a revolutionary energy storage device, may produce two engagements between the electrode materials and the solutions to store energy through the passage of negative and positive ions in the electrolyte. In regards, the storage technology mechanism of the Pseudocapacitor

is that the electrode materials can have and increased storage energy density during the rapid charging and discharging reaction. The electrode material is well known for influencing supercapacitor performance and has become the subject of research. (Guo et al., 2016).

Also, storing electricity generated utilizing solar power is ensuring the regularity, practicability, and dependability of such innovative electricity systems is a serious task. The majority of energy storage devices have not yet reached the expected level of effectiveness. Therefore, it is still tricky to efficiently power massive structures (such as transportation systems and technological equipment that pulse) using solar energy. Hybrid electrical vehicles (HEVs) and its derivatives are the future of eco-friendly transport since they substantially reduce petrol use. EES devices with high energy and power density standards are needed to power these transportation networks. It is impossible without supercapacitors and greater batteries. Despites their large energy densities, these batteries have the lowest power density and cycle stability. Supercapacitors, on the contrary hand, may deliver very high density of power density demands as well as cycle stability cannot be satisfied by any of these technologies alone. (Sundriyal et al., 2018).

The coordination chemistry domain, which comprises of coordination networks with potential voids, includes Metal- Organic Structures (MOFs) and porous coordination polymers (PCPs)(Batten et al., 2013). Over the last several decades, interest in MOFs, an inventive class of porous products made of natural struts that stretch indefinitely through metal nodes, has skyrocketed. Combinatorial chemistry and the wide variety of building blocks make it possible to create structures on demand with properties that are inversely proportional to their structural aspects. Because of these qualities, MOFs are preferred over other congener permeable strong materials like zeolites and activated carbon. In addition to adjusting the size and structure of porous molecules on demand, researchers may manipulate MOFs to their liking. With the revolution of this research, the range of probable applications of MOFs has increased, comprising gas storage /separation, adsorptive separation of industrially demanding liquid mixes, ion-conduction, observation and photonics, heterogeneous catalysis, and drug delivery, etc.(Furukawa, Cordova, O'Keeffe, & Yaghi, 2013; Yuan et al., 2018).

The following overarching causes substantially account for the rise of MOF

chemistry:

Improving accuracy in getting read-out.

Control of host-guest chemistry in various mediums.

Extending knowledge of structural features collected from the database of reported compounds.

More specifically, the latest version of MOFs (soft permeable crystals) has sped up the development of MOFs for host – guest chemistry – based applications (Horike, Shimomura, & Kitagawa, 2009).

Their capacity to perform as operational solids with a high level of precision and selection in visitors' accommodation and identification action have been bolstered by their visitor – responsive structural features. Soft MOFs offer the critical capacity to contain specific active sites, making them useful for a wide range of potentially harmful or important gas or liquid adsorbed applications in the environmental and industrial sectors. And farther to the freedom to design a specific probe / sorbent, MOFs provide the option to pick transduction methods dependent on the application field, such as electromagnetic actions, photonic responses, and naked – eye colorimetry. Plus, further their traditional uses, MOFs have lately shown their value to the detection, collection, to purifying air, water, and soil from pollutants. One of the most pressing challenges facing humanity in the 21st century is reversing the effects of environmental deterioration. This is reflected in the United Nations' list of sustainable development goals (Pelton, 2019). Increased emissions and releases of harmful sorts are linked to shifts in ecological equilibrium, which has driven the pressing need to eradicate pollution. For instance, a 2018 assessment by the world Health Organization (WHO) recommended that more than 90 percent of the world's population breathes toxic air (Howarth et al., 2016). Permeable materials have become great receivers for capturing environmental contaminants or transforming them into harmless chemicals. Although metal-organic frameworks (MOFs) have certain advantages over more traditional porous adsorbents, their use in this field has been capped by the difficulty of achieving stability under operating conditions or the tendency of MOF compounds to disintegrate when exposed to water. An industry-wide initiative to address the problem and encourage expansion is relatively new, and it has already produced tangible results, including the appearance of a growth guarantee with

a substantial time horizon. (Howarth et al., 2016).

In addition to stability, the absence of procedures for forming devices from microcrystalline MOF powders has held back the exploration of MOFs in real-world circumstances. Thus, composites based on MOFs have garnered increased interest, and further study in this area may raise the profile of MOF-based devices(Julien, Mottillo, & Friščić, 2017).

Moreover to these formidable obstacles, toxicity, durability, life-cycle assessment (LCA) research, bulk-scale synthesis, and cost-effectiveness must be considered. They demand careful attention while offering the energy of a newly produced product in real-world situations (Ghosh, 2019; Grande, Blom, Spjelkavik, Moreau, & Payet, 2017).

1.1. Conceptions Necessary to Understand Capacitors

Electrostatic energy may be stored in a capacitor without the need for any chemical processes. A dielectric separates two parallel electrodes (plates) that are arranged on a plane.

That which does not allow electricity to flow through it. When a voltage is applied across the capacitor's electrodes, positive and negative charges migrate, respectively, toward the oppositely polarized electrodes. An electrical circuit may use the voltage supplied by a capacitor once it has been charged. By definition, the capacitance (C), denoted by the SI unit farad (F), is inversely correlated with the potential difference (V) between the electrodes and the electric charge (Q) at each one.

$$C = \frac{\mathrm{Q}}{\mathrm{V}} \qquad \textbf{(1.1)}$$

For a conventional parallel plate capacitor, (C) is inversely proportional to the electrode separation distance and proportionate to the electrode areas (A) and dielectric permittivity (Ɛ), respectively (D), to ensure:

$$\mathrm{C} = \frac{\varepsilon_0 \mathcal{E}_r A}{\mathrm{D}} \qquad \textbf{(1.2)}$$

Where (Ɛ0) is a measure of the dielectric properties of the material (or relative permittivity) between the plates and Ɛr is the permittivity of empty space. Therefore, the three primary elements that affect the capacitance of a capacitor are the dielectric constant, capacitance, and temperature.

The area of the plate is shared by the two electrodes.

The distance between them.

The qualities of the dielectric (inductor) all have a role.

A capacitor's energy density and power density are two of its most distinguishing features. These characteristics may be described as a ratio of one quantity to another, either quantitatively (in terms of specific energy or power) or qualitatively (in terms of volume). The amount of energy E (J) stored in a capacitor is directly proportional to its capacitance because of the inverse connection between the charge Q (C) at each interface and the potential difference V (V):

$$E = {}^{1}/_{2} \times CV2 \quad \textbf{(1.3)}$$

At maximum V, where it is typically restricted by the breakdown strength of the dielectric, the maximum energy is attained.

Power (P) is the rate at which energy is transferred over a certain period of time. To find out what P is for a certain capacitor, The resistance of its internal components (such as current collectors, electrode materials, dielectric/electrolyte, and separators) must be taken into account. These components' resistance is often measured as a whole, equivalent series resistance (ESR) (Ω) is the sum of all of these resistances in a circuit. Since the ESR causes a voltage drop during discharge, it sets the upper bound on the capacitor's maximum energy and power. For capacitors, the maximum power Pmax. It is found by measuring the voltage across the capacitor at matched impedance (where the load resistance is believed to be equal to the capacitor's ESR).

$$P_{max} = \frac{v^2}{4ESR} \quad \textbf{(1.4)}$$

While the peak power produced is still quite high, it is normally lower than Pmax because the resistance of a quality capacitor is often much less than the resistance of the associated load.

1.1.1. Electrode

The electrodes is the most important part of the supercapacitor and the most important part of the technology itself. Typically, electrodes consist of a current collector (Figure 1), an active-material- based paste, a conducting additive, and a binder. In certain cases, additives have been developed to increase the shelf life of a

product.(Ghosh, 2019).

Because capacitance results from the accumulation of purely electrostatic charge at the electrode/electrolyte contact, its magnitude is strongly reliant on the electrode materials' surface area that is available to the electrolyte ions. Supercapacitors have capacitances defined – by electrostatic double layer capacitances or electrochemical pseudocapacitance resulting from reversible reduction and oxidation (redox) operations or intercalation. An example of a hybrid supercapacitor would be one that makes use of both techniques simultaneously.

The advancement of supercapacitor technology continues to focus primarily on the creation of nanostructured electrode materials. Researchers have created and incorporated one-dimensional (1D) printing techniques into the manufacturing method for producing high-performance electrode materials (nanotubes and nanowires), 2-dimensional (2-D) (Nano sheets and Nano discs), Integrating 3D Nano architectures into electrode materials for use in making supercapacitors and batteries, among other applications.(Najib & Erdem, 2019).

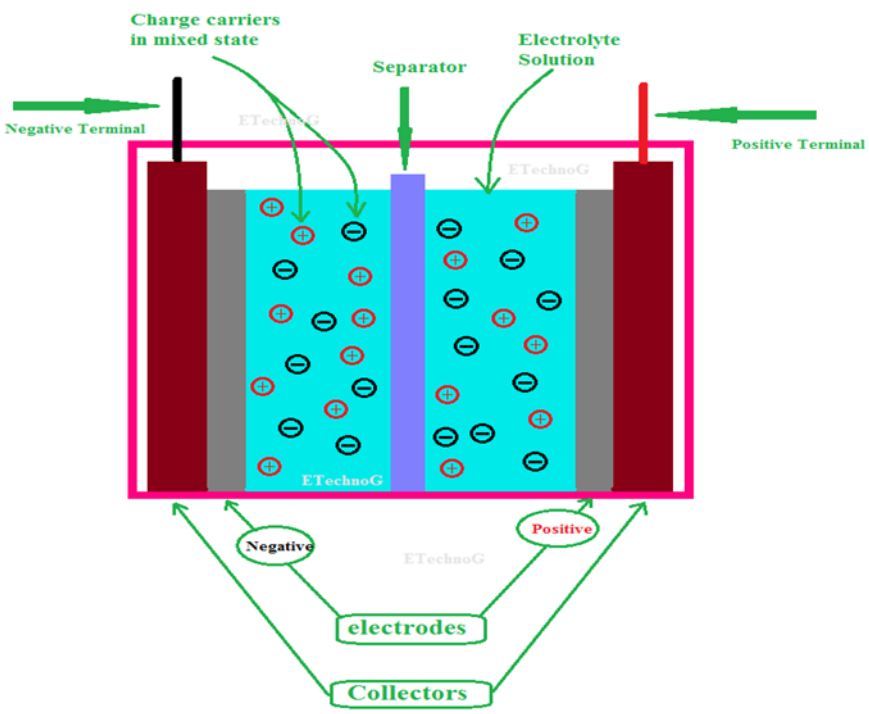

Figure 1.1. Supercapacitor construction

Electrodes in a supercapacitor are typically very thin coverings linked electrically to a metallic current collector. Greater surface areas per units mass and volume, high electrical conductivity, high thermal sustainability, and long-term

chemical stability are all necessary qualities in an electrode. (inertness), and high corrosion resistance.

1.1.2. Electrodes Used in Supercapacitors

As was previously noted, a supercapacitor's capacitance & electrode materials have a crucial role in charge storage. Consequently, a very efficient strategy to Solve issues, it is necessary to develop new materials that are both more capable and more functional than the electrode materials now in use. Essential to the capacitance of the supercapacitor are electrode materials with large surface areas. (Frackowiak et al., 2002; Krawiec et al., 2006)

Because not all of a material's surface area may be used to conduct electricity with different materials measured capacitance when in contact with an electrolyte does not increase linearly with respective surface area. Therefore, it may be more accurate to describe the effect of the electrode capacitance in terms of the electrode's electrochemically active surface area. For specific sections of practical surface.(W. Li et al., 2019; Min, Hu, Li, Wang, & Yang, 2019; Zhao et al., 2020).

It is vital to highlight that the electrodes material's highly porous structure has a function in the electrochemically the amount of surface area that is actively currently performing. Largeot et al. also report that the pore diameters of both the hole size and the size of the ions in an electrolyte (in the case of an ionic liquid electrolyte) were quite near in the electrode materials that produced very high double-layer capacitance, although the presence of either bigger or smaller pores significantly reduced capacitance. (Largeot et al., 2008).

Nevertheless, the capacities of materials with ions is reduced when pore size is increased, since a larger pore size increases the distance travelled between both the center of the ion and the pore wall. According to eqn (2,2), the pores become bigger.

Porous structure and average pore diameter, two components of porosity, are significant parameters for producing high capacity. Concentrated study of one subset of the content.

Consequently, the capacitance depends critically on the electrode's surface area exposed in contact with the electrolyte. There are primarily three types of electrode materials.

(i) Conductive polymers.
(ii) Carbon-based materials.

(iii) Transition metal oxides.

Table 1. A quick evaluation among the most important limitations.

Utilize Components	Surface area	Variation in pore size	Distinctive capacitance	Conductivity	Ranking capability	Stat
Carbon	High	Pore size distribution may be modified in a number of ways.	Low	High	High	Gc
Metal oxides	Low	Constraints on adjusting the distribution of pores	High	Low	Low	P
Metal oxide/conducting polymer combined with carbn=on	Steered by a carbon backbone	Pore size distribution may be modified in a number of ways.	High	Medium to high	High	Gc

1.1.3. Electrochemical Capacitor

Similar to a battery cell, EC needs two electrodes, each of which is negatively charged relative to the other, the electrostatic nature of electrical conduction and separation. Isolation in electron and ion charge are made in a double layer from across electrode interfaces at both electrodes. When the resistivity of the solution and the separator are both zero, the macro equivalent circuit (like a battery) consists of two capacitances connected in series with ohmic resistances. When the electrodes are typically porous matrices with a large surface area, an additional microequivalent circuit is required to model the electrical behavior of the electrode's interior surfaces and electrolyte-containing interstitial spaces (Conway, 2013).

Capacitors that charge and discharge electrochemically are called electrochemical capacitors. If you compare the galvanostatic charging and discharging curves for them to those for standard electrostatic capacitors, you'll see that they're quite similar to a straight line. Film (dielectric), electrolytic, and supercapacitors (ECSCs) are all types of electrochemical capacitors; Electric double – layer capacitors (ELDCs), pseudocapacitors (PsCs), and hybrid capacitors (HCs) are all subsets of ECSCs (HCs). In pulse engineering, capacitors serve as electric power batteries, and in sin-wave current technology, they function as reactive components defined by AC resistance with almost negligible power losses (Bagotsky, Skundin, & Volfkovich, 2015).

1.1.4. Electrochemical capacitor classification

Capacitors can be classified as shown in .

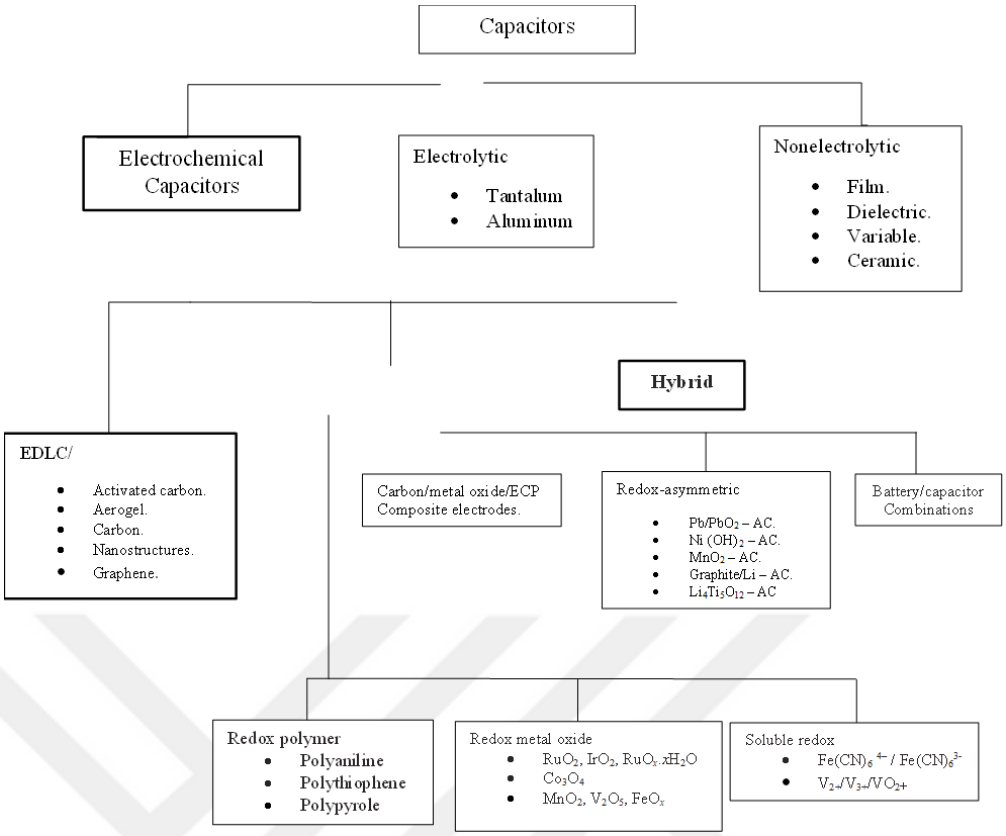

Figure 1.2. Classification of the capacitors

1.2. Quantitative Assessment of Critical Electrochemical Parameters

In this section, we will go through the electrochemical parameters that are used to evaluate the supercapacitor's device performance. Before assembling a supercapacitor, its electrodes are often optimized using a three-electrode method. The suitable electrolyte is present in the associated arrangement of active, reference, and counter electrodes. The final product is an electrolytic capacitor with two electrodes that are arranged symmetrically and asymmetrically over the electrolyte.

1.2.1. Tri-electrode set-up

The following equation is used in conjunction with cyclic voltammograms to get the particular capacitance (Cs in F/g)(Arico, Bruce, Scrosati, Tarascon, & Van Schalkwijk, 2011):

$$C_s = \frac{1}{ms(\Delta V)} \int_{vs}^{vc} I(v)dV \qquad \textbf{(1.5)}$$

Note that **$(\int IdV)$** equals the whole integrated area of the CV curve, where **m** is the mass in grammes of the electrode's active material, **ΔV** = the sum of all voltage swing within the allowed range, and **s** = scan rate in mV/s.

Furthermore, the following equation may be used as a rough approximation for Cs based on the galvanostatic charge – discharge (GCD) curves:

$$C_s = \frac{I \times \Delta t}{\Delta V \times m} \quad (\mathbf{1.6})$$

Where I = the flow of a current in discharge, Δt = duration of discharge (in seconds), and ΔV = total voltage swing in the range under consideration.

GCD curves may also be used to calculate the energy (Es in Wh/kg) and power (Ps in W/kg) densities of the active electrode. (Eqs. (3) and (4)):

$$E_s = \frac{1 \times C_s \times (\Delta V^2)}{2 \times 3.6} \quad (\mathbf{1.7})$$

$$P_s = \frac{4 \times 3600}{\Delta t} \quad (\mathbf{1.8})$$

1.2.2. Set-up using only two electrodes (Equal-sized capacitors)

Using GCD data, we may make an educated guess as to what Cs, for a pair of electrodes of equal size, should be (Eq. (5)(H. Wang, Yi, Chen, & Wang, 2014)).

$$Cs = \frac{4 \times I \times \Delta}{\Delta V \times m} \quad (\mathbf{1.9})$$

Where I = the flow of a current in discharge and m = sum of the active material masses on both electrodes in grammes ($m^+ = m^-$ for Equal-sized capacitors).

Using the following formulas, we can get Es and Ps values of two capacitors of equal capacity:

$$E_s = \frac{1 \times C_s \times (\Delta V^2)}{4 \times 2 \times 3.6} \quad (\mathbf{1.10})$$

$$P_s = \frac{E_s \times 3600}{\Delta t} \quad (\mathbf{1.11})$$

1.3. Nanostructures Based on Metal-Organic Frameworks:

Assembled supercapacitor electrodes; The use of MOFs in energy storage devices like batteries and supercapacitors has recently received much interest(Arico et al., 2011; Hu, Wang, Gao, & Guo, 2010). Selecting electrode materials with a large surface area and enhanced conductivity (Dubal, Gomez-Romero, Sankapal, & Holze, 2015; Wei, Cui, Chen, & Ivey, 2011) is crucial to a supercapacitor's performance, as was discussed before. There are three ways that MOFs can be used during the development of Supercapacitor Technology:

Using pure MOFs, charge storage upon physisorption of electrolyte ions, on the working electrode's inner surface.

Pyrolysis of MOFs in an inert environment to produce conduction nanoporous carbon (NPC) nanostructures while maintaining the high specific surface area attributes.

Changing MOFs/ these MOF treatments cleared the way for the creation of elevated electrode materials used in supercapacitor applications by simultaneously endowing the material with charge – conducting properties and a large specific surface area (Kaur, Kim, Paul, & Deep, 2016; Kumar, Kumar, Bharadwaj, Paul, & Deep, 2014).

1.4. In Detail, What is a MOF?

The chemistry class with the highest rate of growth, MOFs are composed of metal ions and organic molecules arranged in a structured framework. These cutting-edge materials function like sponges, soaking up molecules and releasing them later.

One gram of MOF may equal a surface area as large as 7,000 m2 due to its highly ordered structures. It has the most elevated documented surface area-to-weight ratio ever recorded. The material's high surface area makes it suitable for various chemical processes, such as when molecules bind to it.

MOF can be customized materials we can create to perform specific tasks by combining metal ions with organic molecules in various ways.

Why look at metal-organic frameworks for use in batteries?

MOFs have significant advantages over competing materials due to their adaptability; the benefits of MOFs to humans may be applied in various circumstances, such as electrodes, inside the electrolyte, and as the membrane.

Superior cycle stability, operability over a broad temperature range, shorter charging times, and enhanced security when used as penetration protection.

Utilizing MOFs might be advantageous in several fields. Pharmacy use, like controlling the release of APIs (active pharmaceutical components) or drugs, or protecting APIs from hostile conditions like stomach acid, are two common uses for pharmaceutical metal-organic frameworks (Pharma MOFs). Vaccines and other bioactive compounds may now be delivered with pinpoint accuracy thanks to a modification of metal – organic frameworks. To further the use of MOFs in the pharmaceutical sector, see "Scrubbing the Bathroom," in which Clean room testing

and regulation are only two examples of the many applications of multiple-organic frameworks (MOFs). This includes controlling humidity, filtering out toxic pollutants, and purifying the air.

MOFs improve gas storage in CNG cars and prolong battery life in EVs. MOFs have also been proposed for improved temperature control and cabin air quality.

Innovations in portable production and personal computing

Improvements to batteries made possible by MOFs are already being put to use in mobile electronic devices like laptops, tablets, and smartphones.

Applications for Safe Utility Use: It is possible to employ metal-organic frameworks to detect and neutralize toxic compounds, which might save lives.

1.5. Some Applications of MOF

1.5.1. HKUST-1

HKUST-1 consisting of a metal – organic structure composed of copper in addition to being known as MOF – 199 or CU - BTC. The number of water molecules that the MOF absorbs will cause its characteristic blue hue to shift. The lighter the MOF, the more water molecules will be adsorbed (Hendon & Walsh, 2015).

Among the many different types of metal-organic frameworks, HKUST-1 is one of the most investigated (Furukawa et al., 2014; Todaro et al., 2016).

Implementations

- Detection and separation of gases (e.g. CO_2)
- Catalysis
- The ability to conduct ions and electricity
- Antifungal
- The process of taking in and storing gas (carbon dioxide CO, nitrogen N_2, oxygen O_2, hydrogen H_2).

Characteristics

- Formula: $C_{18}H_6Cu_3O_{12}$
- Surface area: 1100 – 2200 m2/gr (BET)

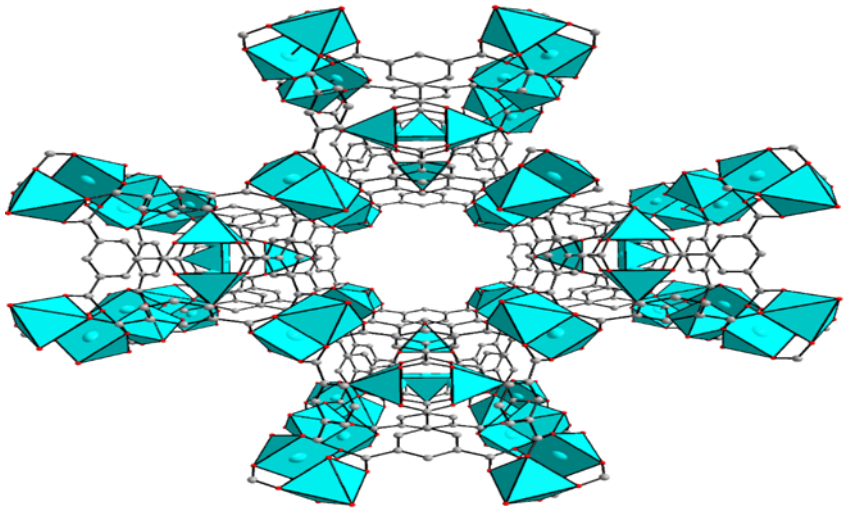

Figure 1.3.Structure of HUHUST 1

1.5.2. Zirconium-Based UiO-66

Zirconium-based UiO-66 consisting of a metal – organic structure that has a high porosity. In addition, it has good stability in water and is resistant to a wide range of acids. It does not decompose until temperatures beyond 500 degrees (Acetone, benzene and DMF). UiO-66 demonstrates a high degree of versatility in both its functionalization and its use(Stassen et al., 2016; Chenghong Wang, Liu, Chen, & Li, 2015).

Implementation:-

- Absorption of water
- Arsenic removal from wastewater
- Dechlorination, or the process of purifying water by eliminating ammonia
- Storage by adsorption on a porous surface Substances: Carbon dioxide (CO2), Nitrogen (N2), Methane (CH4) (N2)
- To identify gases (electrochemical sensor)
- Conversion of nerve gas to a harmless form (chemical warfare) Transportation of Meds

Characteristics

- Formula: $Zr_6O_4(OH)_4(BDC)_6$,
- Surface area: up to 1300m^2/g ,Pore size: 7.4 Å, 8.4 Å

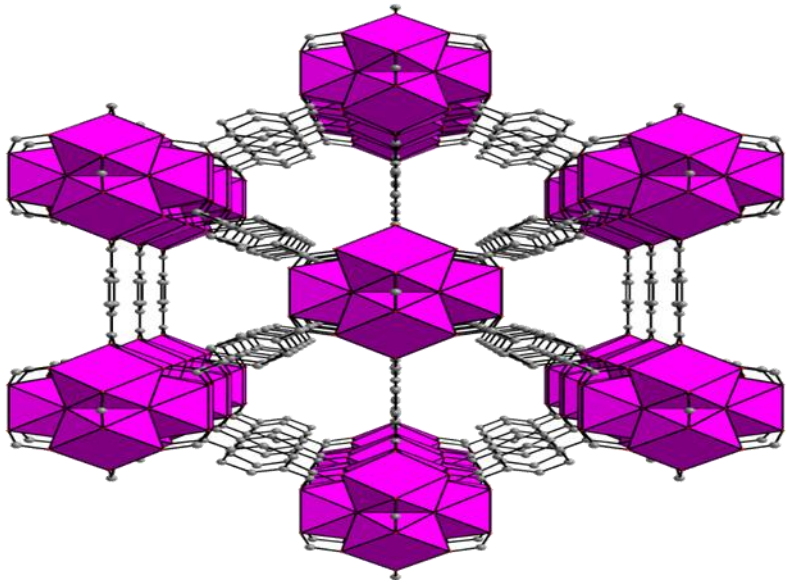

Figure 1.4. Structure of Zirconium-based UiO-66

1.5.3. MOF UiO-67

MOF UiO-67 compared to UiO-66, the pore diameters of the metal-organic framework known as UiO-67, based on zirconium, are much more significant. This is because BPDC (UiO-67) has a more extensive structure than BDC (which is shorter) (UiO-66).(Øien-Ødegaard et al., 2016; G. Zhong, Liu, & Zhang, 2018).

Implementation

Keeping gases on hand by adsorption and storage:

- Dubbed "the silent killer," carbon dioxide (CO2)
- Hydrogen (H2)
- Methane (CH4)

Agents of chemical warfare are neutralized or detoxicated (nerve gas)

Catalyst

- The molecular driver of biomolecules
- Clinical imaging

Characteristics

- The chemical composition is as follows: Zr6O4(OH)4(BPDC)6.
- Estimated Surface Area: 1970 m2/gr (BET)

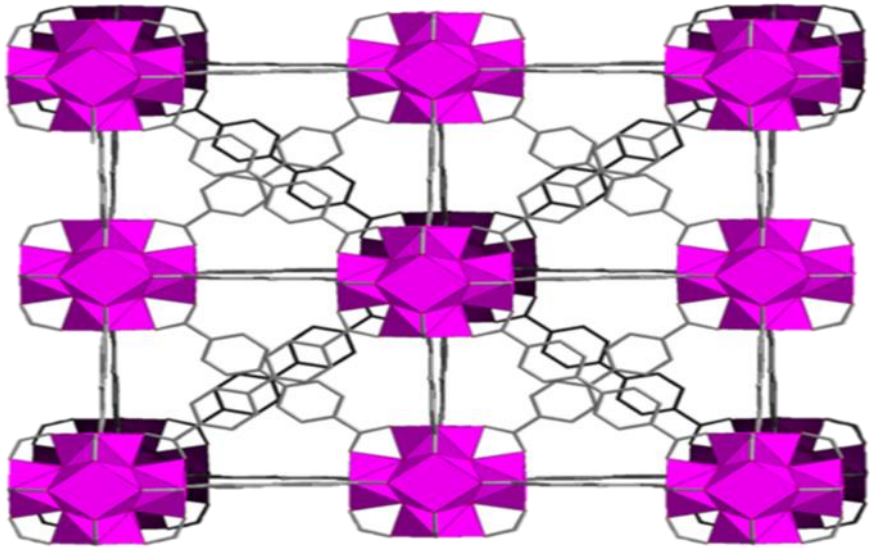

Figure 1.5. Structure of MOF UiO-67

1.5.4. ZIF 67

ZIF 67 Mainly due to the fact that it has such a massive surface, an unusually big size for the pores, with the additional perk of being easily functionalized, imidazole zeolite frameworks (ZIFs) have garnered a significant amount of interest as a newly discovered category of crystalline porous materials. Creating novel methods to control ZIF growth and composition is essential.(Wen, Zhang, Yu, Yi, & Guo, 2021)

It is highly valued for its catalytic uses and is therefore a functional and helpful chemical. With its high oxygen evolution reaction (OER) productivity, Nano-ZIF has gained appeal as a promising electrode material in recent years, leading to fresh insights into the research of electrolyzed water. Here, we'll take a look back at the history of ZIF-67 adding cations to alter a material's morphology, anion doping, co-doping, methods of making up new combinations in a formula (metal oxide, phosphide, sulfide, selenide, and telluride), in tandem with atomic-scale catalysis (core-shell, hollow, and array structures). In addition, By incorporating this information, the study of actual active sites is given more priority with DFT calculations and examines the difficulties and potential of electrocatalysts based on ZIF-67. To our knowledge, this is the first complete account of ZIF-67 and its variants' ground-breaking contribution in guiding OER research.

Multiple MOF variants have been developed to stimulate the oxygen release mechanism, but their poor stability has limited their practical applicability. ZIF, on the other hand, is very stable because to its unusual structure (ZIF-67's skeleton structure

is made up of metal Co^{2+} ions and N atoms of 2-methylimidazole, which hybridize with the four-coordinate SOD structure to make tetrahedral structural units).

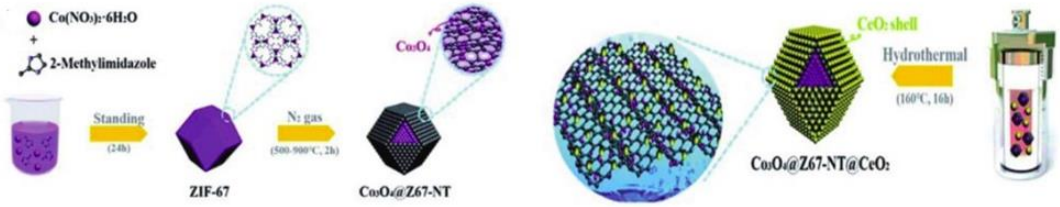

Figure 1.6. Synthesis route for the Co_3O_4@Z67-NT@CeO_2 composites

Furthermore, ZIF is a very desirable subtype. There are a number of benefits associated with this material, including its high porosity, thermal and chemical resilience, wide surface area, and customizable porous structure.

Table 2.A review of the efficiency of porous carbon electrodes generated from ZIF in the level of supercapacitors.

ZIF precursor	ZIF derived electrode	Area of a given surface with precision ($m^2 g^{-1}$)	Electrolyte	Capacitance	Scan rate/current Density	Ref
ZIF-69	Activated carbon	2264	0.5 M H2SO4	168 F g^{-1}	5 mV s^{-1}	(Q. Wang et al., 2013)
ZIF-8	3D carbon	655	1 M H2SO4	206 F g^{-1}	100 mV s^{-1}	(Amali, Sun, & Xu, 2014)
ZIF-8	Nanoporous carbon	1523	1 M H2SO4	251 F g^{-1}	5 mV s^{-1}	(Salunkhe et al., 2014)
ZIF-8	Nanoporous carbon/GO	1304	1 M H2SO4	246 F g^{-1}	2 mV s^{-1}	(Martín-Jimeno et al., 2017)
ZIF-8	Porous carbon	n/a	6 M KOH	185 F g^{-1}	5 mV s^{-1}	(Hou et al., 2014)
ZIF-8	Porous carbon	1823	1 M H2SO4	219 F g^{-1}	5 mV s^{-1}	(Young et al., 2016)
ZIF-8	N-doped porous carbon	943	6 M KOH	285.8 F g^{-1}	0.1 A g^{-1}	(S. Zhong, Zhan, & Cao, 2015)
ZIF-8	N-doped porous carbon sheets	1190	1 M H2SO4	290 F g^{-1}	1 A g^{-1}	(Huang, Hao, Zhang, & Chen, 2018)
ZIF-8	Carbon Nanofiber	314	1 M H2SO4	322 F g^{-1}	1A g^{-1}	(Chaohai Wang et al., 2017)
ZIF-8/GO	Porous carbon	280	1 M H2SO4	238 F g^{-1}	1 A g^{-1}	(C. Li et al., 2014)
ZIF-8/67	Nanoporous carbon	415	0.5 M H2SO4	286 F g^{-1}	2.5 A g^{-1}	(Kim et al., 2018)
ZIF-67	Carbon polyhedron/nanotube	1723	6 M KOH	190 F g^{-1}	0.5 A g^{-1}	(Gao, Zhou, Ma, & Li, 2018)
ZIF-8/MWCNT	Porous carbon	569	1 M H2SO4	326 F g^{-1}	1 A g^{-1}	(Y. Wang et al., 2016)
ZIF-8/MWCNT	MWCNT/nanoporous carbon	928	1 M H2SO4	293.4 F g^{-1}	5 mV s^{-1}	(X. Li et al., 2017)
ZIF-8/CNT	ZnO/porous carbon/CNT	600	1 M Na2SO4	250 F g^{-1}	1 A g^{-1}	(Y. Zhang et al., 2016)
ZIF-8/PANI	Core–shell nanoporous carbon	1610	1 M H2SO4	236 F g^{-1}	1 A g^{-1}	(Salunkhe, Tang, et al., 2016)
ZIF-67	Nanoporous carbon	943	0.5 M H2SO4	240 F g^{-1}	20 mV s^{-1}	(Liu, Xu, Shao, & Jiang, 2020)
ZIF-67	N-doped porous carbon	683	1 M H2SO4	305 F g^{-1}	1 A g^{-1}	(Lei et al., 2017)
ZIF-7/glucose	Porous carbon	783	6 M KOH	228 F g^{-1}	0.1 A g^{-1}	(P. Zhang, Sun, Shen, & Cao, 2014)
ZIF-67	Nanoporous carbon/CoS	521.4	2 M KOH	677 F g^{-1}	10 mV s^{-1}	(Ahmad, Iqbal, & Noor, 2019)
ZIF-67	BIC carbon	1361	1 M KOH	119 F g^{-1}	0.5 Ag	(Deng et al., 2017)
ZIF-8	Hollow carbon spheres	920	6 M KOH	280 F g^{-1}	1 A g^{-1}	(Xin et al., 2017)
ZIF-8	NiAl LDH/porous carbon	383	1 M KOH	1370 F g^{-1}	1 A g^{-1}	(Han, Cheng, Zhang, Zhang, & Wang, 2018)
ZIF-8	Nanoporous carbon	1873	2 M NEt4BF4/PC	21 F g^{-1}	10 mV s^{-1}	(Salunkhe, Young, et al., 2016)

2. MATERIALS AND METHOD

2.1. Materials and Chemicals

In the synthesis, Sigma-Aldrich 2-methylimidazole, 1-vinylimidazole, 2-methylimidazole, terefitalic acid, 2,5-dihydroxyterephthalic acid, N,N-dimethylformamide, ethanol and $Co(NO_3)_2.6H_2O$ were used as received.

2.2. Devices Used

The devices used for synthesis and characterization are explaned. Stuart and MTOPS make magnetic stirrers were used for solving metal salt in DMF. PARR 4744 model general purpose 45 mL PTFE lined vessel was used as high pressure reactors. Fourier transform infrared spectroscopy, powder X-ray diffraction and potentiostat were used for characterization. The equipmets used are explained briefly in the following sections.

2.2.1. Magnetic Stirrers

Magnetic stirrers were used to prepare solutions. Stoichometeric ratio of metal salts, linkers and solvents mixed to get clear solutions before heating in high pressure reactors. A typical magnetic stirring hotplate is seen in Figure 2.1.

Figure 2.1. Stuart CB162 magnetic stirring hotplate

2.2.2. 4744 General Purpose Acid Digestion Vessel

General purpose acid digestion vessel was used as high pressure reactor for solvothermal synthesis where reaction mixtures are heated above the boiling point of the solvent. Hydrothermal Synthesis synthesis of 2D coordination compounds were carried out in Parr high pressure reactors as seen in Figure 2.2. Clear solutions of metal salt, linkers and solvent were poured in vessel and heated at 120 °C.

Figure 2.2. 4744 General purpose acid digestion vessel

2.2.3. Fourier Transform Infrared Spectroscopy

Perkin Elmer FT-IR 8000 spectrophotometer was used by using ATR attachment at frequencies between 400–4000 cm^{-1} in order to make structural analyzes by confirming functional groups, Figure 2.3.

Figure 2.3. Perkin Elmer FT-IR 8000

2.2.4. Powder X-ray Diffraction

XRD analyses were performed for identification of the phases obtainedd. Powder x-ray data were collected using Panalytical/Emperian Powder X-ray diffractometer. The X-ray sourse is Co K_{alpha}, wavelength 1.79 Å. Scan range and step size were from 5.0 to 90 and 0.0131303 degree, respectively.

Figure 2.4. Panalytical / Emperian Powder X-ray diffractometer

2.3. Electrochemical Characterization

The electrochemical characterization was carried out using a conventional 3-electrode system with Ni foam /Co_2O_3-CC- as the working electrode, Ag/AgCl as the reference electrode, and 4.5 cm^2 platinum (Pt) as the counter electrode in 1 M Na_2SO_4 and 6 M KOH electrolyte. Gamry Reference 600 potentiostat was used to measure CV of the samples.

Figure 2.5.Gamry Reference 600 potentiostat/galvanostat/ZRA

2.4. Synthesis of MOS's

Metal–organic framework (MOF)-derived hybrids can be used as energy storage materials because of their high surface area and plentiful redox sites (Ma et al., 2022). In this work, a cobalt-based 2D two different coordination polymers were tried to synthesised.

ZIF-67 is 3D coordination polymer, widely used as supercapacitor electrode material and consists of cobalt ion (Co^{2+}) and 2-methylimidazolate anions (Ma et al., 2022; Wen et al., 2021; Zhao et al., 2020). In order to get 2-methylimidazole and 1-vinylimidazole mixed ligand 2D coordination compound, cobalt ion (Co^{2+}), 2-methylimidazole and 1-vinylimidazole were mixed in teflon lined autoclave and heated at 120 °C for 24 hours. Co^{2+}:2-mim:1-vim mol ratios were 1:2:2, 1:2:4 and 1:2:8.

MOF-5 is most widely worked 3D coordination polymer and consists of zinc ion (Zn^{2+}) and tereftalate anion. In order to get terephtalic acid (BDC) and 1-vim mixed ligand 2D coordination compound, cobalt ion (Co^{2+}), BDC and 1-vim were mixed in teflon lined autoclave and heated at 120 °C for 24 hours. Co^{2+}:tere:1-vim mol ratios were 1:1:1 and 1:1:2.

2.5. Electrode Preperation

Cobalt ion (Co^{2+}), 2-methylimidazole and 1-vinylimidazole compositions did not give any 2D coordination compounds but ZIF-67. (Co^{2+}), BDC and 1-vim composition gave $[Co_3(BDC)_3(1\text{-vim})_2$. $[Co_3(BDC)_3(1\text{-vim})_2$ was pyrolyzed under argon atmosphere to obtain Co_3O_4. Conductive carbon (CC) was used to improve

conductivity. 60% [$Co_3(BDC)_3(1\text{-}vim)_2$, 20% CC and 30% Polyvinylidene fluoride (PVDF) were mixed for cathode preparation and named as composition 1

Two different compositions were prepared for pyrolyzed [$Co_3(BDC)_3(1\text{-}vim)_2$. In the second cathode composition, 60% Pyrolyzed MOF and 40% PVDF were mixed and named as composition 2. In the third composition, CC also added in order to improve conductivity. 40% Pyrolyzed MOF, 20%CC and 20% PVDF were mixed to prepare composition 3. The electrochemical characterization was carried out using a conventional 3-electrode system with Ni foam /Co_2O_3-CC and Ni foam /MOF-CC- as the working electrode, Ag/AgCl as the reference electrode, and 4.5 cm^2 platinum (Pt) as the counter electrode in 1 M Na_2SO_4 and 6 M KOH electrolyte.

3. RESULTS AND DISCUSSION

3.1. 2D MOF synthesis

Cobalt ion (Co^{2+}), 2-methylimidazole and 1-vinylimidazole compositions did not give any 2D coordination compounds but ZIF-67. The Structure of ZIF-67 is seen in Figure 3.1 (J. Zhang, Zhang, Yu, Xiao, & Hong, 2015).

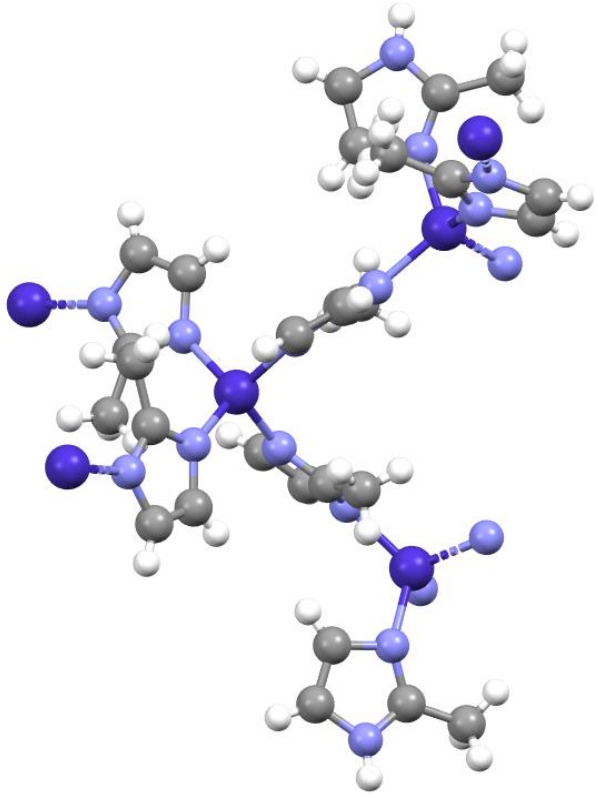

Figure 3.1. Structure of MOF-67 from CCDC no: 7222297 (J. Zhang et al., 2015)

Co^{2+}, BDC and 1-vim mixtures gave only one composition, $[Co_3(BDC)_3(1\text{-}vim)_2$, as seen in Figure 3.2. $[Co_3(BDC)_3(1\text{-}vim)_2$ has already beed reported before but its supercapacitor performance was not studied (Yıldız, 2014). Slightly different method was applied fort he synthesis. 2mmol $Co(NO_3)_2.6H_2O$ and 2 mmol H_2BDC were dissolved in 10 mL DMF and 5 mL absolute ethanol. After mixing , 4 mmol 1-vim was added dropwise to $Co(NO_3)_2.6H_2O$ and H_2BDC solutions. Thereafter, the solution was moved to 40 mL teflon lined autoclave and heated at 120 C for 24 hours. Finally, obtained solid washed with absolute ethanol three times and dried at 50 °C.

3.2. 2D MOF Characterization by XRD

In the Structure, there are two different Co^{2+} environment, tetrahedral and

octahedral. The coordination geometry around 1-Vim coordinated Co^{2+} is tetrahedral, Figure 3.2. However, octahedral Co^{2+} is coordinated by BDC oxygen atoms.

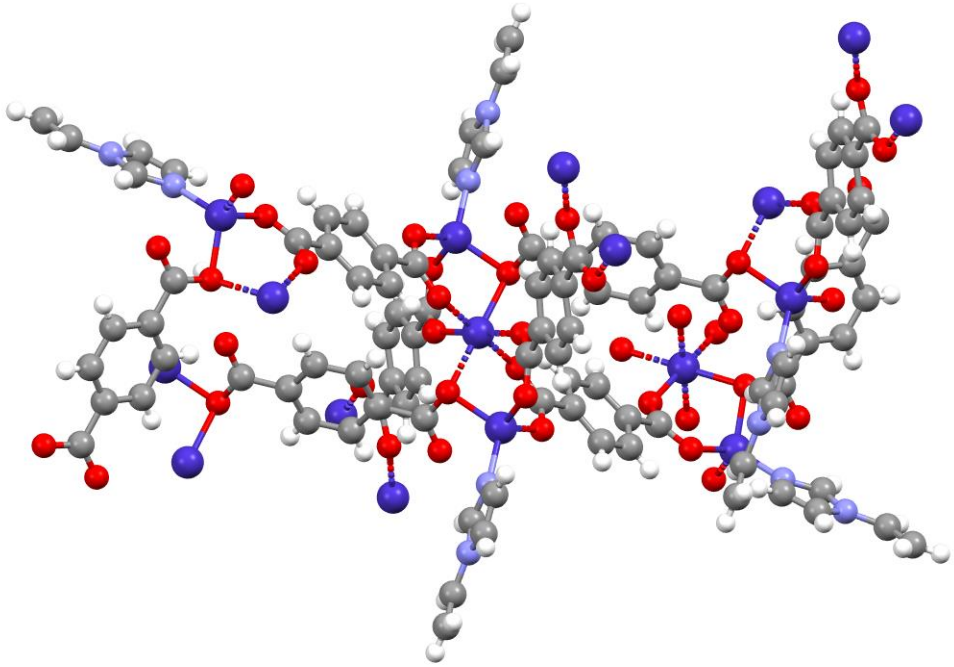

Figure 3.2. Molecular view of [Co3(BDC)3(1-vim)2] syntheised(Yıldız, 2014)

Packing structure of is seen in Figure 3.3. Terephthalate ligands can be seen along c axis. 1-vim ligands can be seen along a axis.

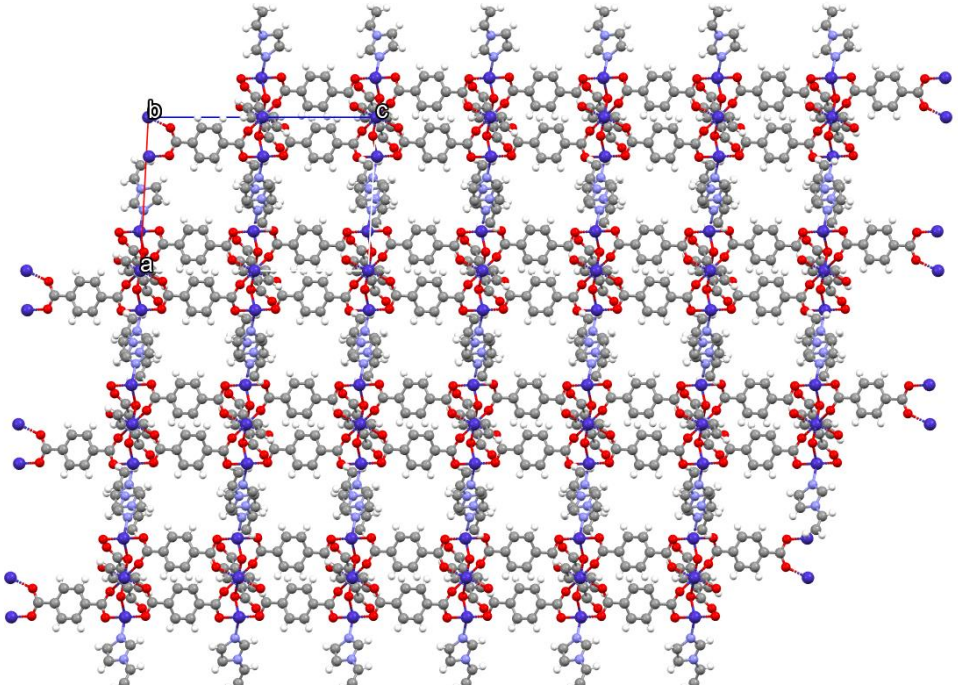

Figure 3.3. Packing structure of the $[Co_3(BDC)_3(1\text{-vim})_2]n$, down to b axis.

Powder x-ray results confirmed the synthesis of $[Co_3(BDC)_3(1\text{-vim})_2]_n$, Figure 3.4.

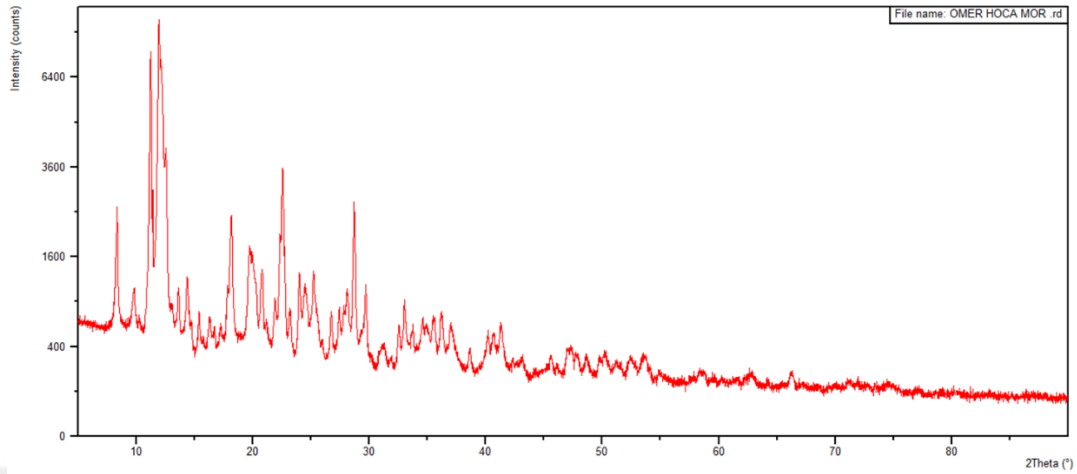

Figure 3.4. Powder X-ray data of $[Co_3(BDC)_3(1\text{-vim})_2]_n$

Single crystal data is reported in a MSc thesis (Yıldız, 2014). The crystal information file (CIF) was not published elsewhere. To compare experimental powder data with single crystal data, powder X-ray data was calculated using CIF data. It is seen that single crystal and powder crystals obtained in this work is same, Figure 3.5

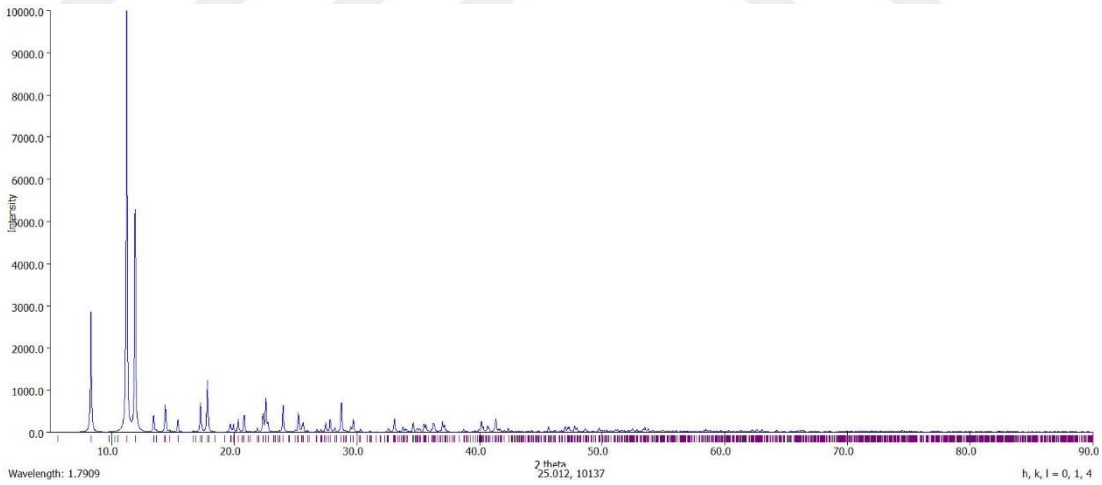

Figure 3.5. Calculated powder pattern of $[Co_3(BDC)_3(1\text{-vim})_2]_n$

3.3. Thermal analysis of $[Co_3(BDC)_3(1\text{-vim})_2]_n$

Thermal analysis (TA) of $[Co_3(BDC)_3(1\text{-vim})_2]_n$ can be seen in Figure 3.6. TA results confirmed that $[Co_3(BDC)_3(1\text{-vim})_2]$ decomposes in three main stages and the finally Co_3O_4 formation was observed. The formation of Co_3O_4 was correlated by powder X-ray data.

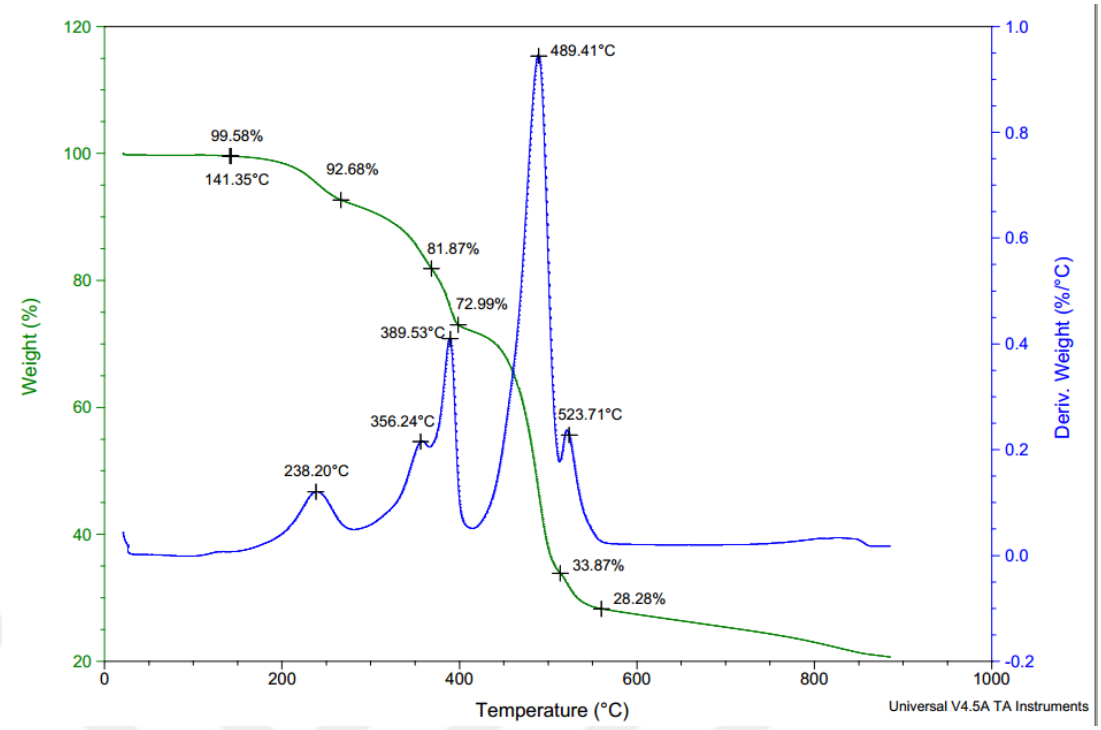

Figure 3.6.Thermal analysis of $[Co_3(BDC)_3(1\text{-vim})_2]_n$

3.4. FTIR

Characteristic bands for 1-vim and BDC are observed at 3134cm−1 (C–H ring stretching), 2939 cm^{-1} (C–H and CH_2 stretching on the main chain), 1651 cm^{-1} (C=C ring stretching), 1568 (C=O), 1502 cm−1 (C–C and C=N ring stretching), 1278, 1228 and 1091 cm^{-1} (C–H ring bending and C–N ring stretching), 1067 ($C=CH_2$)

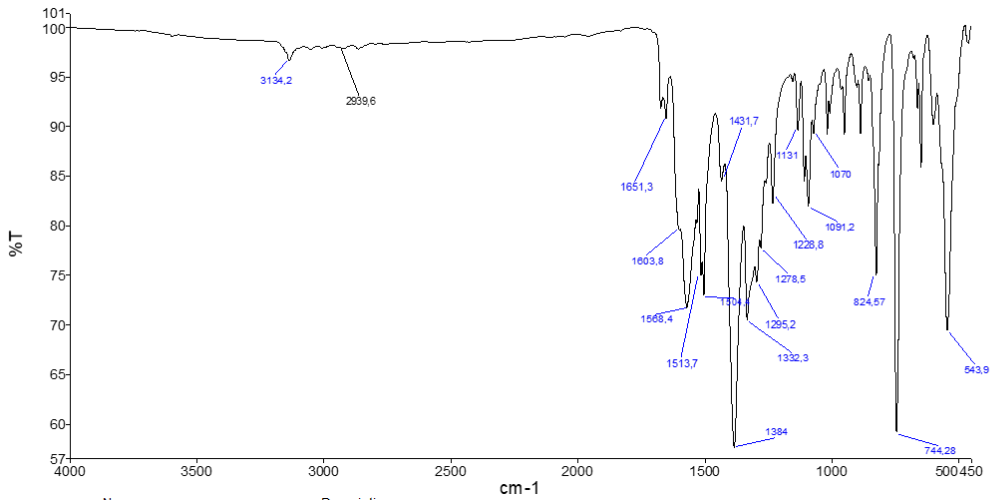

Figure 3.7.FTIR data of $[Co_3(BDC)_3(1\text{-vim})_2]_n$

3.5. Pyrolysis

$[Co_3(BDC)_3(1\text{-vim})_2]_n$ was pyrolyzed under argon atmosphere to obtain Co_3O_4.

TA data revealed that decomposition of the $[Co_3(BDC)_3(1\text{-}vim)_2]_n$ was completed at 550 °C. Therefore pyrolysis temperature was selected as 600 °C.

The powder X-ray data of Co_3O_4 obtained by pyrolysis of $[Co_3(BDC)_3(1\text{-}vim)_2]_n$ is seen in Figure 3.8. The data was successfully indexed using PDF Card - 00-042-1467. The peak at 48.82 ° belongs to carbonous material.

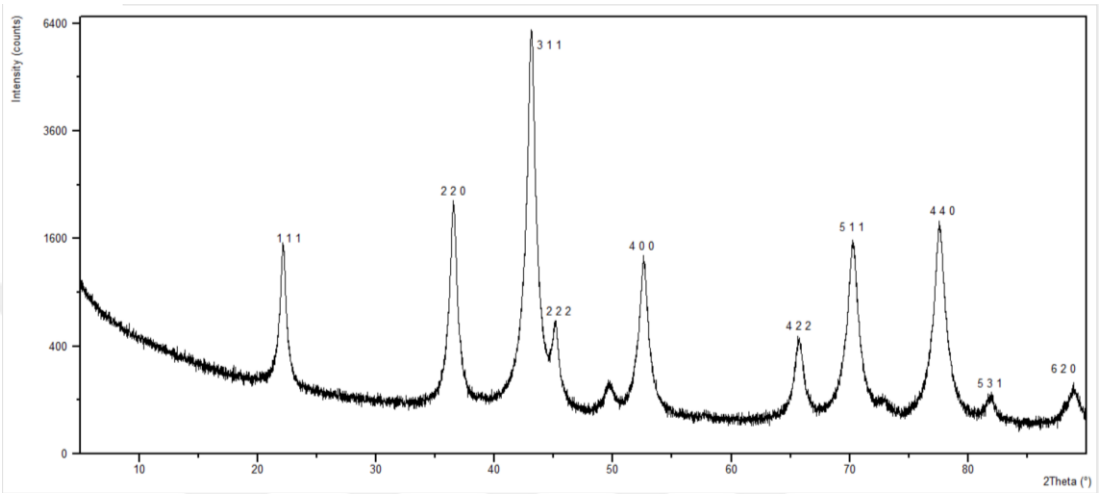

Figure 3.8. Pyrolysis of $[Co_3(BDC)_3(1\text{-}vim)_2]_n$ at 600 C

3.6. Electrochemical Characterization

Polyvinylidene fluoride was used as the binder material and and conductive carbon was used to improve the conductivity in making of electrodes for supercapacitors. Electrochemical performance of $[Co_3(BDC)_3(1\text{-}vim)_2]$n and Co_3O_4 were studied by the cyclic voltammetry and electrochemical impedance spectroscopy in a three- electrode system in 6 M KOH and 1 M Na_2SO_4 electrolyte.

Working electrode was prepared by loading electroactive materials on to 2 cm^2 Ni foam. Three different composition were prepared. For Composition 1, 60% $[Co_3(BDC)_3(1\text{-}vim)_2]_n$, 20% CC and 30% PVDF were mixed. 60% Pyrolysed MOF and 40% PVDF were mixed and named as composition 2. In the third composition, CC also added in order to improve conductivity. 40% Pyrolyzed MOF, 20%CC and 20% PVDF were mixed to prepare composition 3.

The electrochemical characterization was carried out using a conventional 3-electrode system with Ni foam /Co_3O_4-CC- as the working electrode, Ag/AgCl as the reference electrode, and 4.5 cm^2 platinum (Pt) as the counter electrode in 1 M Na_2SO_4 and 6 M KOH electrolyte.

CV's of composition 1 in Na_2SO_4 at at scan rates of 10, 100, 500 and 1000 mV/s are seen in Figure 3.9. MOF_1_Na2SO4_1, MOF_1_Na2SO4_2, MOF_1_Na2SO4_3 and MOF_1_Na2SO4_4 are CV's of composition 1 at 10, 100, 500 and 1000 mV/s, respectively. The CV area is increased with increasing scan rate. Cathodic and anodic peaks are not seen at high scan rates.

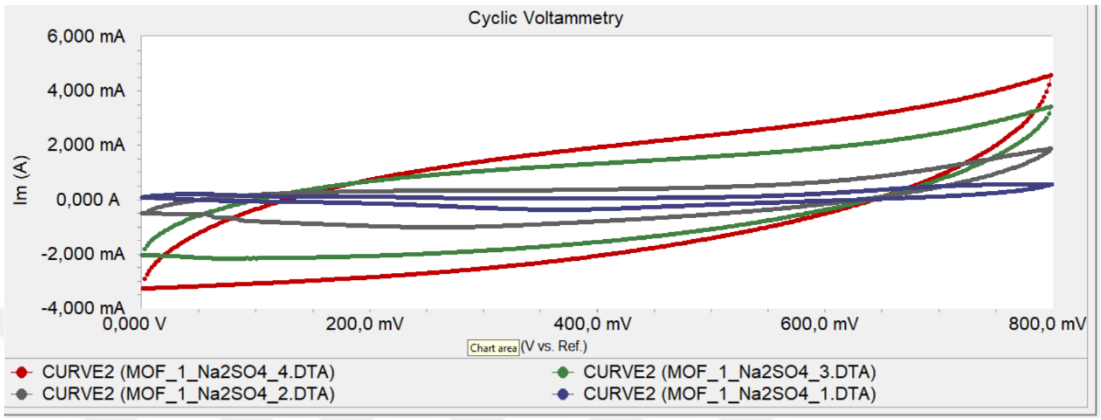

Figure 3.9. CV's of composition 1 at scan rates of 100, 500 and 1000 mV/s in Na_2SO4

CV's of composition 1 in KOH at at scan rates of 10, 100, 500 and 1000 mV/s are seen in Figure 3.10. MOF_CC_KOH_1, MOF_CC_KOH_2, MOF_CC_KOH_3 and MOF_CC_KOH_4 are CV of composition 1 at 10, 100, 500 and 1000 mV/s scan rates, respectively. The CV area is increased with increasing scan rate. Cathodic and anodic peaks are not seen.

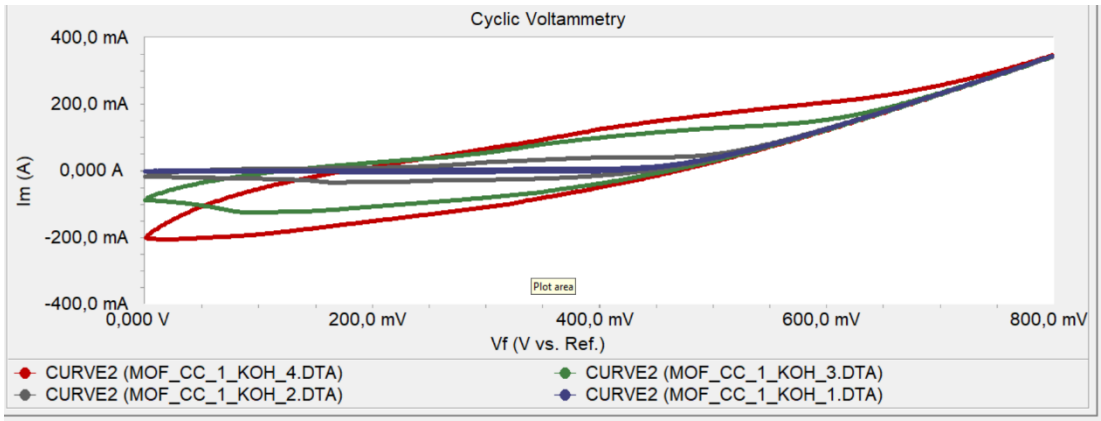

Figure 3.10. CV of composition 1 at scan rates of 10,100, 500 and 1000 mV/s in KOH

Composition 2 is the pyrolyzed product of $[Co_3(BDC)_3(1\text{-vim})_2]_n$ at 600 °C. Powder X-ray data of composition 2 reveals that it contains mainly Co_3O_4 and most probably small amount of carbonous material. Composition 2 contains small amount of conductive carbonous material occurred during pyrolysis. CV's of composition 2 at

scan rates of 10, 100, 500 and 1000 mV/s in KOH are seen in Figure 3.11. Pyrolized_600_2_KOH_1, Pyrolized_600_2_KOH_2, Pyrolized_600_2_KOH_3 and Pyrolized_600_2_KOH_3 in Figure 3.11 are CVs of composition at scan rates of 10, 100, 500 and 1000 mV/s in KOH. The maximum potential in a scan rate at 10 mV/s is 800 mV. Since there is no area above 500 mV, other scans were carried out between 0 to 500 mV. Anodic and cathodic peaks can be seen.

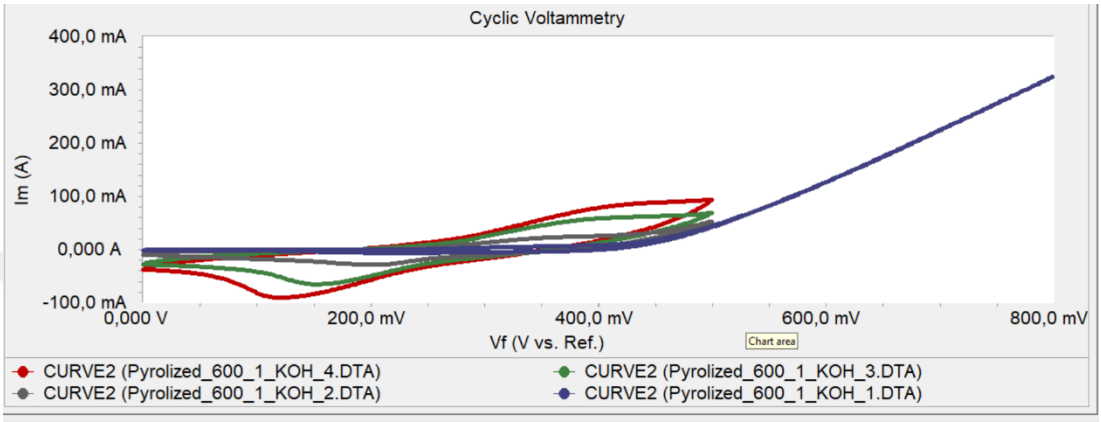

Figure 3.11. CV's of composition 2 at scan rates of 100, 500 and 1000 mV/s in KOH

Composition 3 contains the pyrolyzed product of $[Co_3(BDC)_3(1\text{-vim})_2]_n$ at 600 °C and CC. CC was added to composition 3 to improve the conductivity. Pyrolized600_cc_Na2SO4_1, Pyrolized600_cc_Na2SO4_2, Pyrolized600_cc_Na2SO4_3 and Pyrolized600_cc_Na2SO4_4 are the CV's of composition 3 at scan rates of 10, 100, 500 and 1000 mV/s in in Na_2SO_4 solution, Figure 3.12.

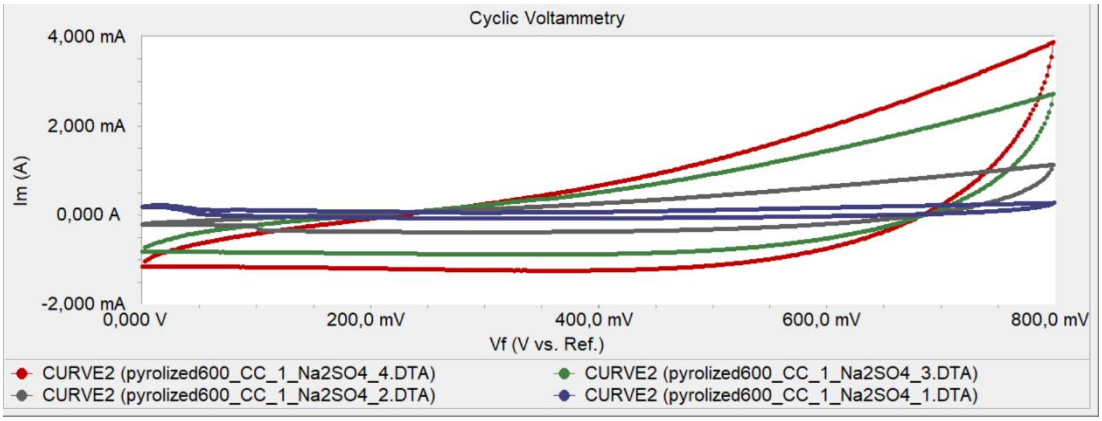

Figure 3.12. CV's of composition 3 at scan rates of 10, 100, 500 and 1000 mV/s in in Na_2SO_4 solution

Pyrolized600_CC_KOH_1, Pyrolized600_CC_KOH_2, Pyrolized600_CC_KOH_3 and Pyrolized600_CC_KOH_4 are the CV's of

composition 3 at scan rates of 10, 100, 500 and 1000 mV/s in in KOH solution, Figure 3.13. Small cathodic peak can be seen at 400 mV. It is more obvious at high scan rates.

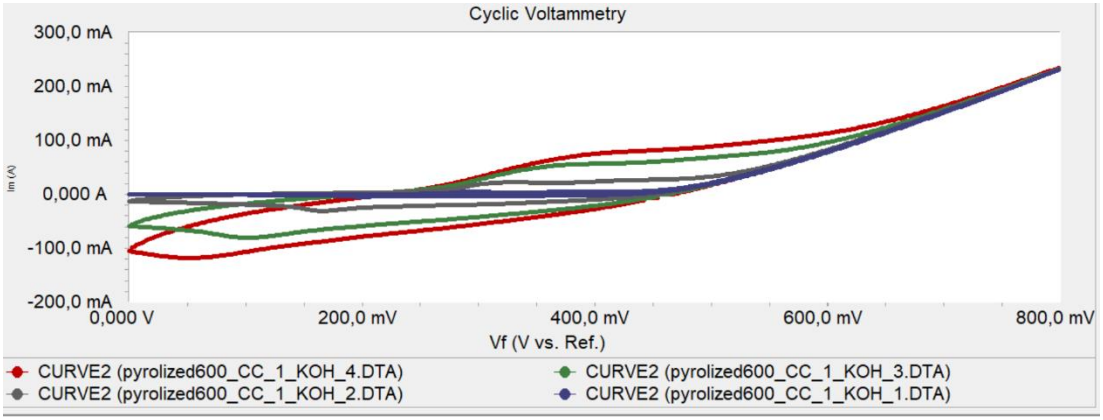

Figure 3.13. CV's of composition 3 in KOH solution, at 10, 100, 500 and 1000 mV/s scan rate

Cp of the prepared samples were calculated using the formula of area/(mass x scan speed x potential windows. Area of the CV's were calculated using Origin program. Cp's of the MOF in Na_2SO_4 are below 5 F/g. These values are too low comparing to literature values. Cp's of the MOF in KOH are comparable. But the Cp values are different for different scan ranges. Cp's of the compositions are decreasing with increasing scan speed as expected.

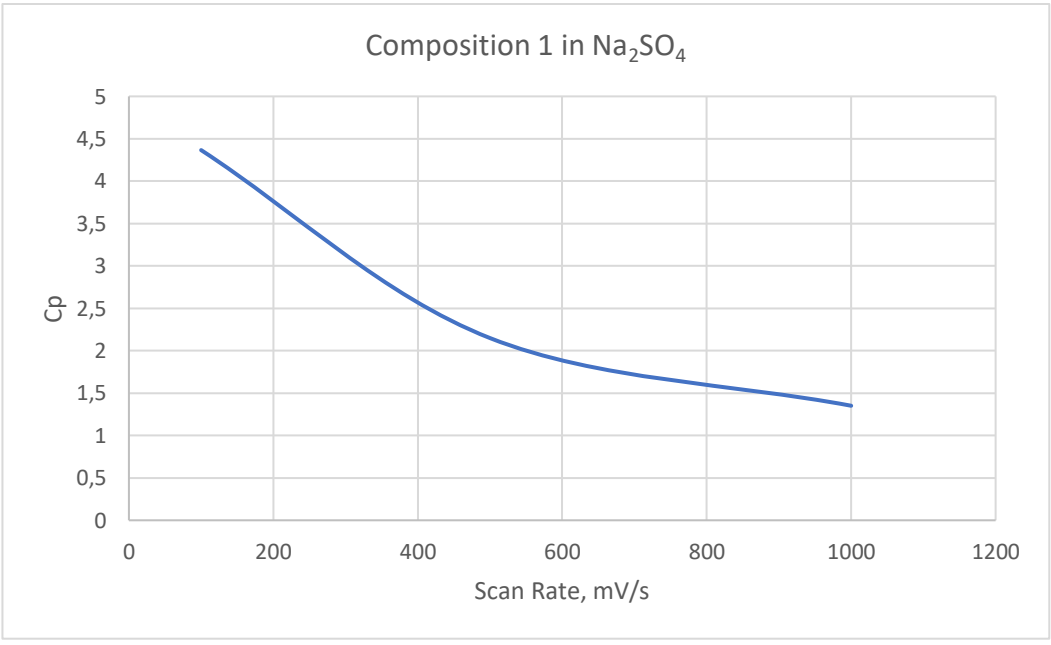

Figure 3.14. Cp values of composition 1 in Na_2SO_4 at 100, 500 and 1000 mv/s scan rates

Composition 1 in KOH has Cp value of 451 at 100 mV/s scan rate. This is the highest value obtained in this work. Cp values of composition 1 in KOH at 100, 500

and 1000 mV/s scan rates are seen in Figure 3.15.

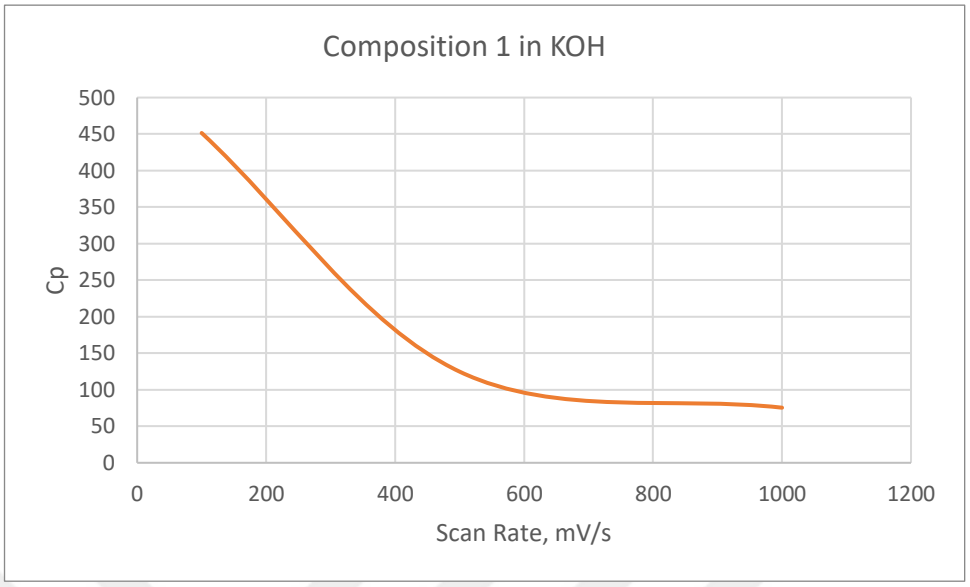

Figure 3.15. Cp values of composition 1 in KOH at 100, 500 and 1000 mv/s scan rates

Cp values of composition 2 in KOH at 100, 500 and 1000 mV/s scan rates are seen in Figure 3.16

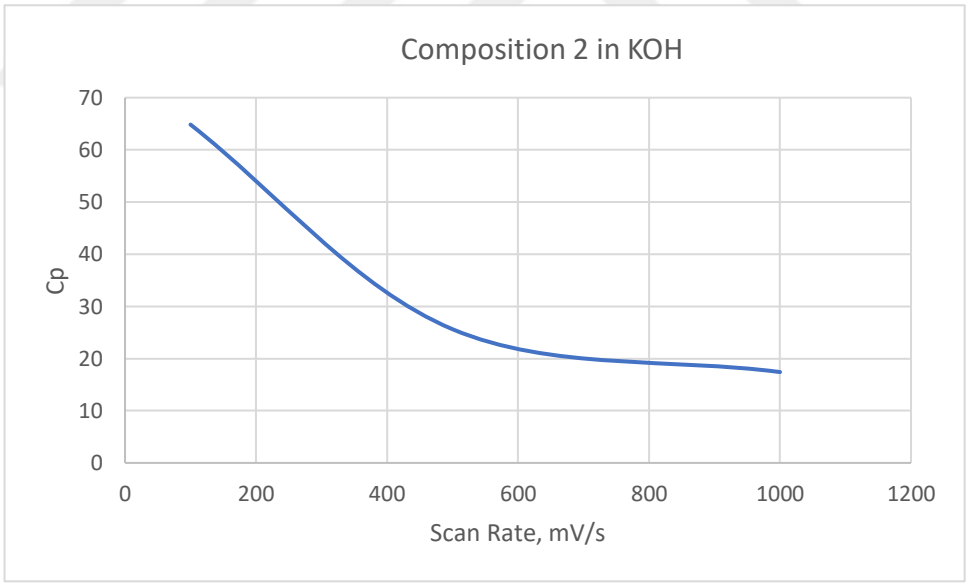

Figure 3.16. Cp values of composition 2 in KOH at 100, 500 and 1000 mv/s scan rates

Cp values of composition 3 in Na_2SO_4 and KOH at 100, 500 and 1000 mv/s scan rates are seen in Figure 3.17and Figure 3.18. Cp values of composition 3 in KOH has high Cp values comparing to Na_2SO_4.

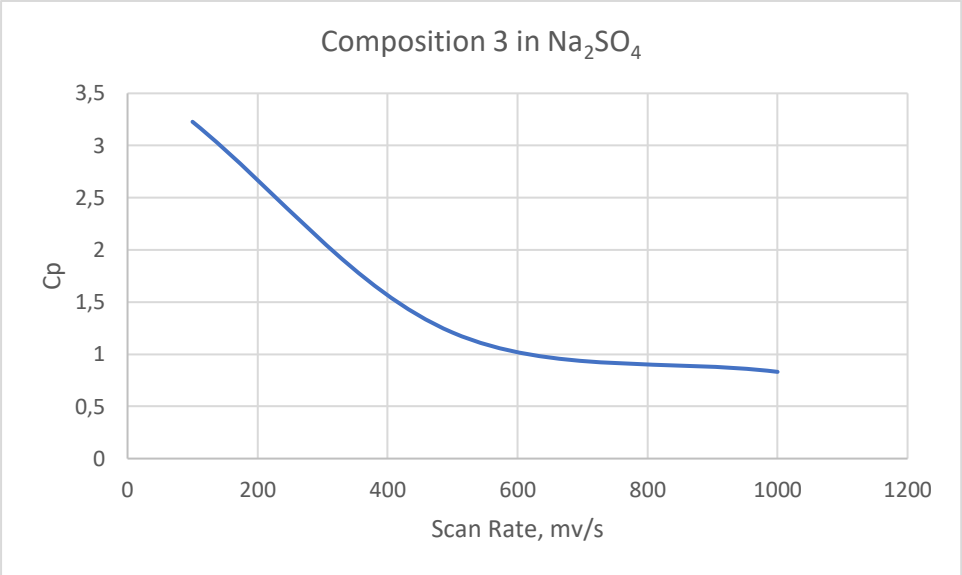

Figure 3.17. Cp values of composition 3 in Na_2SO_4 at 100, 500 and 1000 mv/s scan rates

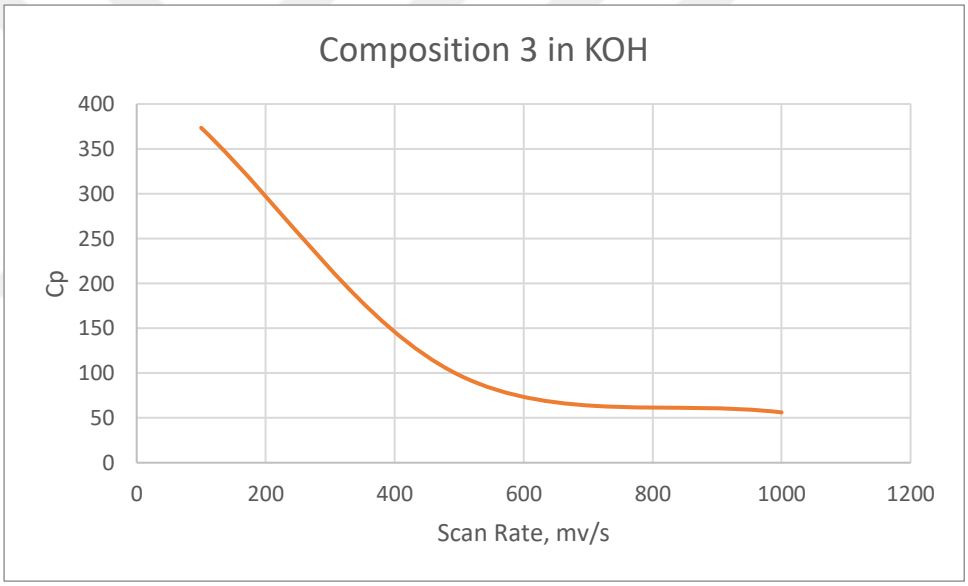

Figure 3.18. Cp values of composition 3 in KOH at 100, 500 and 1000 mv/s scan rates

Table 3. Cp of prepared samples

Sample Name	Area (AV)	Scan rate (V/s)	Potential windows (V1-V2)	mass (g/cm^2)	Cp
Composition 1 in Na_2SO_4_2	0,001135288	0,1	0,8	0.0033	4,36649
Composition 1 in Na_2SO_4_3	0,002793877	0,5	0,8	0.0033	2,149136
Composition 1 in Na_2SO_4_4	0,003512976	1,0	0,8	0.0033	1,351145
Composition 1 in KOH_2	0,13365118	0,1	0,8	0.0037	451,5243
Composition 1 in KOH_3	0,184646165	0,5	0,8	0.0037	124,7609
Composition 1 in KOH_4	0,223236332	1,0	0,8	0.0037	75,41768
Composition 2 in KOH_2	0,014524653	0,1	0,5	0,0028	64,8422
Composition 2 in KOH_3	0,028698165	0,5	0,5	0,0028	25,62336
Composition 2 in KOH_4	0,03899346	1,0	0,5	0,0028	17,40779
Composition 3 in Na_2SO_4_2	0,00072300	0,1	0,8	0,0028	3,227494
Composition 3 in Na_2SO_4_3	0,001352635	0,5	0,8	0,0028	1,20771
Composition 3 in Na_2SO_4_4	0,001861438	1,0	0,8	0,0028	0,830999
Composition 3 in KOH_2	0,088139924	0,1	0,8	0,0030	373,4743
Composition 3 in KOH_3	0,115250871	0,5	0,8	0,0030	97,67023
Composition 3 in KOH_4	0,132386126	1,0	0,8	0,0030	56,09582

4. CONCLUSION

A cobalt-based coordination polymer was prepared under standard solvothermal conditions using $Co(NO_3)_2$.6H2O as metal precursor, BDC and 1-VIM as organic ligands and N,N-dimethylformamide (DMF) and ethanol as solvents. A coordination polymer $[Co_3(BDC)_3(1\text{-}vim)_2]$ was obtained and characterized by TA, PXRD and FTIR.

TA results confirmed that $[Co_3(BDC)_3(1\text{-}vim)_2]$ decomposes in three main stages and the finally Co_3O_4 formation was observed at 550 °C. The pyrolysis temperature was chosen as 600 °C since Co_3O_4 formation was observed at 550 °C.

Vibration of vinily, carboxyl and C—H were observed in FTIR results. Characteristic bands for 1-vim and BDC are observed at 3134cm−1 (C–H ring stretching), 2939 cm^{-1} (C–H and CH_2 stretching on the main chain), 1651 cm^{-1} (C=C ring stretching), 1568 (C=O), 1502 cm−1 (C–C and C=N ring stretching), 1278, 1228 and 1091 cm^{-1} (C–H ring bending and C–N ring stretching), 1067 ($C=CH_2$).

Powder X-ray data was used to characterise crystal structures formed. Theoretical powder x-ray pattern was calculated from single crystal data of $[Co_3(BDC)_3(1\text{-}vim)_2]_n$. Experimental and calculated powder x-ray data of $[Co_3(BDC)_3(1\text{-}vim)_2]_n$ were compared and the synthesis of $[Co_3(BDC)_3(1\text{-}vim)_2]_n$ was proven.

Cobalt-based active material, Co_3O_4, was obtained by thermal treatments at 600 °C and characterized by powder X-ray diffraction. The data was successfully indexed using PDF Card - 00-042-1467 and the formation of Co_3O_4 was proven.

Polyvinylidene fluoride was used as the binder material and and conductive carbon was used to improve the conductivity in making of electrodes for supercapacitor electrodes. Electrochemical performance of $[Co_3(BDC)_3(1\text{-}vim)_2]$ and Co_3O_4 were studied by the cyclic voltammetry in a three- electrode system in KOH and Na_2SO_4 electrolyte. Working electrode was prepared by loading electroactive materials on to 2 cm^2 Ni foam. Three different compositions were prepared. For Composition 1, 60% $[Co_3(BDC)_3(1\text{-}vim)_2]_n$, 20% CC and 30% PVDF were mixed. 60% Pyrolyzed MOF and 40% PVDF were mixed and named as composition 2. In the third composition, CC also added in order to improve conductivity. 40% Pyrolysed MOF, 20%CC and 20% PVDF were mixed to prepare composition 3.

Cp of the prepared samples were calculated using the formula of area/(mass x scan speed x potential windows. Cp's of the MOF in Na_2SO_4 are very low comparing to literature values. Cp's of the MOF in KOH are comparable. Cp's of the compositions are decreasing with increasing scan speed as expected. Cp values of composition 3 in KOH has high Cp values comparing to Na_2SO_4. Composition 1 in KOH has Cp value of 451 at 100 mV/s scan rate. This is the highest value obtained in this work.

REFERENCES

Ahmad, R., Iqbal, N., & Noor, T. (2019). Development of ZIF-Derived Nanoporous Carbon and Cobalt Sulfide-Based Electrode Material for Supercapacitor. *Materials, 12*(18), 2940.

Amali, A. J., Sun, J.-K., & Xu, Q. (2014). From assembled metal–organic framework nanoparticles to hierarchically porous carbon for electrochemical energy storage. *Chemical communications, 50*(13), 1519-1522.

Arico, A. S., Bruce, P., Scrosati, B., Tarascon, J.-M., & Van Schalkwijk, W. (2011). Nanostructured materials for advanced energy conversion and storage devices. *Materials for sustainable energy: a collection of peer-reviewed research and review articles from Nature Publishing Group*, 148-159.

Bagotsky, V. S., Skundin, A. M., & Volfkovich, Y. M. (2015). *Electrochemical power sources: batteries, fuel cells, and supercapacitors*: John Wiley & Sons.

Batten, S. R., Champness, N. R., Chen, X.-M., Garcia-Martinez, J., Kitagawa, S., Öhrström, L., OKeeffe, M., Suh, M. P., & Reedijk, J. (2013). Terminology of metal–organic frameworks and coordination polymers (IUPAC Recommendations 2013). *Pure and Applied Chemistry, 85*(8), 1715-1724.

Conway, B. E. (2013). *Electrochemical supercapacitors: scientific fundamentals and technological applications*: Springer Science & Business Media.

Deng, X., Zhu, S., Li, J., Ma, L., He, F., Liu, E., He, C., Shi, C., Li, Q., & Zhao, N. (2017). Ball-in-cage nanocomposites of metal–organic frameworks and three-dimensional carbon networks: synthesis and capacitive performance. *Nanoscale, 9*(19), 6478-6485.

Dubal, D. P., Gomez-Romero, P., Sankapal, B. R., & Holze, R. (2015). Nickel cobaltite as an emerging material for supercapacitors: an overview. *Nano Energy, 11*, 377-399.

Frackowiak, E., Delpeux, S., Jurewicz, K., Szostak, K., Cazorla-Amoros, D., & Beguin, F. (2002). Enhanced capacitance of carbon nanotubes through chemical activation. *Chemical Physics Letters, 361*(1-2), 35-41.

Furukawa, H., Cordova, K. E., O'Keeffe, M., & Yaghi, O. M. (2013). The chemistry and applications of metal-organic frameworks. *Science, 341*(6149), 1230444.

Furukawa, H., Gandara, F., Zhang, Y.-B., Jiang, J., Queen, W. L., Hudson, M. R., & Yaghi, O. M. (2014). Water adsorption in porous metal–organic frameworks and related materials. *Journal of the American Chemical Society, 136*(11), 4369-4381.

Gao, T., Zhou, F., Ma, W., & Li, H. (2018). Metal-organic-framework derived carbon polyhedron and carbon nanotube hybrids as electrode for electrochemical supercapacitor and capacitive deionization. *Electrochimica Acta, 263*, 85-93.

Ghosh, S. K. (2019). *Metal-organic frameworks (MOFs) for environmental applications*: Elsevier.

Grande, C. A., Blom, R., Spjelkavik, A., Moreau, V., & Payet, J. (2017). Life-cycle assessment as a tool for eco-design of metal-organic frameworks (MOFs). *Sustainable materials and technologies, 14*, 11-18.

Guo, S., Zhu, Y., Yan, Y., Min, Y., Fan, J., Xu, Q., & Yun, H. (2016). (Metal-Organic Framework)-Polyaniline sandwich structure composites as novel hybrid electrode materials for high-performance supercapacitor. *Journal of Power Sources, 316*, 176-182.

Han, B., Cheng, G., Zhang, E., Zhang, L., & Wang, X. (2018). Three dimensional hierarchically porous ZIF-8 derived carbon/LDH core-shell composite for high performance supercapacitors. *Electrochimica Acta, 263*, 391-399.

Hendon, C. H., & Walsh, A. (2015). Chemical principles underpinning the performance of the metal–organic framework HKUST-1. *Chemical Science, 6*(7), 3674-3683.

Horike, S., Shimomura, S., & Kitagawa, S. (2009). Soft porous crystals. *Nature chemistry, 1*(9), 695-704.

Hou, S., Zhang, G., Zeng, W., Zhu, J., Gong, F., Li, F., & Duan, H. (2014). Hierarchical core–shell structure of ZnO nanorod@ NiO/MoO2 composite nanosheet arrays for high-performance supercapacitors. *ACS applied materials & interfaces, 6*(16), 13564-13570.

Howarth, A. J., Liu, Y., Li, P., Li, Z., Wang, T. C., Hupp, J. T., & Farha, O. K. (2016). Chemical, thermal and mechanical stabilities of metal–organic frameworks. *Nature Reviews Materials, 1*(3), 1-15.

Hu, J., Wang, H., Gao, Q., & Guo, H. (2010). Porous carbons prepared by using metal–organic framework as the precursor for supercapacitors. *Carbon, 48*(12), 3599-3606.

Huang, J., Hao, F., Zhang, X., & Chen, J. (2018). N-doped porous carbon sheets derived from ZIF-8: preparation and their electrochemical capacitive properties. *Journal of Electroanalytical Chemistry, 810*, 86-94.

Julien, P. A., Mottillo, C., & Friščić, T. (2017). Metal–organic frameworks meet scalable and sustainable synthesis. *Green Chemistry, 19*(12), 2729-2747.

Kaur, R., Kim, K.-H., Paul, A., & Deep, A. (2016). Recent advances in the photovoltaic applications of coordination polymers and metal organic frameworks. *Journal of Materials Chemistry A, 4*(11), 3991-4002.

Kim, J., Young, C., Lee, J., Park, M.-S., Shahabuddin, M., Yamauchi, Y., & Kim, J. H. (2018). Correction: CNTs grown on nanoporous carbon from zeolitic imidazolate frameworks for supercapacitors. *Chemical communications, 54*(47), 6073-6073.

Krawiec, P., Kramer, M., Sabo, M., Kunschke, R., Froede, H., & Kaskel, S. (2006). Improved Hydrogen Storage in the Metal-Organic Framework Cu3 (BTC) 2. *Advanced Engineering Materials, 8*(4), 293-296.

Kumar, P., Kumar, P., Bharadwaj, L. M., Paul, A., & Deep, A. (2014). Luminescent nanocrystal metal organic framework based biosensor for molecular recognition. *Inorganic Chemistry Communications, 43*, 114-117.

Largeot, C., Portet, C., Chmiola, J., Taberna, P.-L., Gogotsi, Y., & Simon, P. (2008). Relation between the ion size and pore size for an electric double-layer capacitor. *Journal of the American Chemical Society, 130*(9), 2730-2731.

Lei, Y., Gan, M., Ma, L., Jin, M., Zhang, X., Fu, G., Yang, P., & Yan, M. (2017). Synthesis of nitrogen-doped porous carbon from zeolitic imidazolate framework-67 and phenolic resin for high performance supercapacitors. *Ceramics International*, *43*(8), 6502-6510.

Li, C., Hu, C., Zhao, Y., Song, L., Zhang, J., Huang, R., & Qu, L. (2014). Decoration of graphene network with metal–organic frameworks for enhanced electrochemical capacitive behavior. *Carbon*, *78*, 231-242.

Li, W., Islam, N., Azam, S., Xu, Z., Warzywoda, J., & Fan, Z. (2019). ZIF-67-derived edge-oriented graphene clusters coupled with carbon nanotubes containing encapsulated Co nanoparticles for high-frequency electrochemical capacitors. *Sustainable Energy & Fuels*, *3*(11), 3029-3037.

Li, X., Hao, C., Tang, B., Wang, Y., Liu, M., Wang, Y., Zhu, Y., Lu, C., & Tang, Z. (2017). Supercapacitor electrode materials with hierarchically structured pores from carbonization of MWCNTs and ZIF-8 composites. *Nanoscale*, *9*(6), 2178-2187.

Liu, Y., Xu, X., Shao, Z., & Jiang, S. P. (2020). Metal-organic frameworks derived porous carbon, metal oxides and metal sulfides-based compounds for supercapacitors application. *Energy Storage Materials*, *26*, 1-22.

Ma, Z., Li, J., Ma, R., He, J., Song, X., Yu, Y., Quan, Y., & Wang, G. (2022). The methodologically obtained derivative of ZIF-67 metal–organic frameworks present impressive supercapacitor performance. *New Journal of Chemistry*, *46*(15), 7230-7241.

Martín-Jimeno, F., Suarez-Garcia, F., Paredes, J., Enterria, M., Pereira, M., Martins, J., Figueiredo, J., Martinez-Alonso, A., & Tascón, J. (2017). A "nanopore lithography" strategy for synthesizing hierarchically micro/mesoporous carbons from ZIF-8/graphene oxide hybrids for electrochemical energy storage. *ACS applied materials & interfaces*, *9*(51), 44740-44755.

Min, X., Hu, X., Li, X., Wang, H., & Yang, W. (2019). Synergistic effect of nitrogen, sulfur-codoping on porous carbon nanosheets as highly efficient electrodes for capacitive deionization. *Journal of colloid and Interface science*, *550*, 147-158.

Najib, S., & Erdem, E. (2019). Current progress achieved in novel materials for supercapacitor electrodes: mini review. *Nanoscale Advances*, *1*(8), 2817-2827.

Øien-Ødegaard, S., Bouchevreau, B., Hylland, K., Wu, L., Blom, R., Grande, C., Olsbye, U., Tilset, M., & Lillerud, K. P. (2016). UiO-67-type metal–organic frameworks with enhanced water stability and methane adsorption capacity. *Inorganic chemistry*, *55*(5), 1986-1991.

Pelton, J. (2019). UN Sustainable Development Goals for 2030. *Handbook of Small Satellites: Technology, Design, Manufacture, Applications, Economics and Regulation*, 1-30.

Salunkhe, R. R., Kamachi, Y., Torad, N. L., Hwang, S. M., Sun, Z., Dou, S. X., Kim, J. H., & Yamauchi, Y. (2014). Fabrication of symmetric supercapacitors based on MOF-derived nanoporous carbons. *Journal of Materials Chemistry A*, *2*(46), 19848-19854.

Salunkhe, R. R., Tang, J., Kobayashi, N., Kim, J., Ide, Y., Tominaka, S., Kim, J. H., & Yamauchi, Y. (2016). Ultrahigh performance supercapacitors utilizing core–

shell nanoarchitectures from a metal–organic framework-derived nanoporous carbon and a conducting polymer. *Chemical Science, 7*(9), 5704-5713.

Salunkhe, R. R., Young, C., Tang, J., Takei, T., Ide, Y., Kobayashi, N., & Yamauchi, Y. (2016). Correction: A high-performance supercapacitor cell based on ZIF-8-derived nanoporous carbon using an organic electrolyte. *Chemical communications, 52*(93), 13620-13620.

Stassen, I., Bueken, B., Reinsch, H., Oudenhoven, J., Wouters, D., Hajek, J., Van Speybroeck, V., Stock, N., Vereecken, P., & Van Schaijk, R. (2016). Towards metal–organic framework based field effect chemical sensors: UiO-66-NH 2 for nerve agent detection. *Chemical Science, 7*(9), 5827-5832.

Sundriyal, S., Kaur, H., Bhardwaj, S. K., Mishra, S., Kim, K.-H., & Deep, A. (2018). Metal-organic frameworks and their composites as efficient electrodes for supercapacitor applications. *Coordination Chemistry Reviews, 369*, 15-38.

Todaro, M., Buscarino, G., Sciortino, L., Alessi, A., Messina, F., Taddei, M., Ranocchiari, M., Cannas, M., & Gelardi, F. M. (2016). Decomposition process of carboxylate MOF HKUST-1 unveiled at the atomic scale level. *The Journal of Physical Chemistry C, 120*(23), 12879-12889.

Wang, C., Liu, C., Li, J., Sun, X., Shen, J., Han, W., & Wang, L. (2017). Electrospun metal–organic framework derived hierarchical carbon nanofibers with high performance for supercapacitors. *Chemical communications, 53*(10), 1751-1754.

Wang, C., Liu, X., Chen, J. P., & Li, K. (2015). Superior removal of arsenic from water with zirconium metal-organic framework UiO-66. *Scientific reports, 5*(1), 1-10.

Wang, D.-G., Liang, Z., Gao, S., Qu, C., & Zou, R. (2020). Metal-organic framework-based materials for hybrid supercapacitor application. *Coordination Chemistry Reviews, 404*, 213093.

Wang, H., Yi, H., Chen, X., & Wang, X. (2014). Asymmetric supercapacitors based on nano-architectured nickel oxide/graphene foam and hierarchical porous nitrogen-doped carbon nanotubes with ultrahigh-rate performance. *Journal of Materials Chemistry A, 2*(9), 3223-3230.

Wang, Q., Xia, W., Guo, W., An, L., Xia, D., & Zou, R. (2013). Functional zeolitic-imidazolate-framework-templated porous carbon materials for CO2 capture and enhanced capacitors. *Chemistry–An Asian Journal, 8*(8), 1879-1885.

Wang, Y., Chen, B., Zhang, Y., Fu, L., Zhu, Y., Zhang, L., & Wu, Y. (2016). ZIF-8@ MWCNT-derived carbon composite as electrode of high performance for supercapacitor. *Electrochimica Acta, 213*, 260-269.

Wei, W., Cui, X., Chen, W., & Ivey, D. G. (2011). Manganese oxide-based materials as electrochemical supercapacitor electrodes. *Chemical society reviews, 40*(3), 1697-1721.

Wen, H., Zhang, S., Yu, T., Yi, Z., & Guo, R. (2021). ZIF-67-based catalysts for oxygen evolution reaction. *Nanoscale, 13*(28), 12058-12087.

Xin, L., Chen, R., Liu, Q., Liu, J., Li, Z., Li, R., & Wang, J. (2017). Composites of hierarchical metal–organic framework derived nitrogen-doped porous carbon and interpenetrating 3D hollow carbon spheres from lotus pollen for high-

performance supercapacitors. *New Journal of Chemistry, 41*(21), 12835-12842.

Yıldız, Z. (2014). *Tereftalik Asit ve Vinilimidazol İçeren Koordinasyon Bileşiklerinin Sentezi, Karakterizasyonu ve Hidrojen Depolama Kapasiteleri.* (Yüksek Lisans). Ondokuz Mayıs Üniversitesi, Samsun.

Young, C., Salunkhe, R. R., Tang, J., Hu, C.-C., Shahabuddin, M., Yanmaz, E., Hossain, M. S. A., Kim, J. H., & Yamauchi, Y. (2016). Zeolitic imidazolate framework (ZIF-8) derived nanoporous carbon: the effect of carbonization temperature on the supercapacitor performance in an aqueous electrolyte. *Physical Chemistry Chemical Physics, 18*(42), 29308-29315.

Yuan, S., Feng, L., Wang, K., Pang, J., Bosch, M., Lollar, C., Sun, Y., Qin, J., Yang, X., & Zhang, P. (2018). Stable metal–organic frameworks: design, synthesis, and applications. *Advanced Materials, 30*(37), 1704303.

Zhang, J., Zhang, T., Yu, D., Xiao, K., & Hong, Y. (2015). Transition from ZIF-L-Co to ZIF-67: a new insight into the structural evolution of zeolitic imidazolate frameworks (ZIFs) in aqueous systems. *Crystengcomm, 17*(43), 8212-8215.

Zhang, P., Sun, F., Shen, Z., & Cao, D. (2014). ZIF-derived porous carbon: a promising supercapacitor electrode material. *Journal of Materials Chemistry A, 2*(32), 12873-12880.

Zhang, Y., Lin, B., Wang, J., Tian, J., Sun, Y., Zhang, X., & Yang, H. (2016). All-solid-state asymmetric supercapacitors based on ZnO quantum dots/carbon/CNT and porous N-doped carbon/CNT electrodes derived from a single ZIF-8/CNT template. *Journal of Materials Chemistry A, 4*(26), 10282-10293.

Zhao, L., Yang, A., Wang, A., Yu, H., Dai, J., & Zheng, Y. (2020). ZIF-67 derived Co, Fe, Ni co-doped porous carbon as an efficient electrocatalyst for hydrogen evolution reaction. *Journal of Porous Materials, 27*(6), 1685-1690.

Zhong, G., Liu, D., & Zhang, J. (2018). Incorporation of Functional Groups Expands the Applications of UiO-67 for Adsorption, Catalysis and Thiols Detection. *ChemistrySelect, 3*(25), 7066-7080.

Zhong, S., Zhan, C., & Cao, D. (2015). Zeolitic imidazolate framework-derived nitrogen-doped porous carbons as high performance supercapacitor electrode materials. *Carbon, 85*, 51-59.

CURRICULUM VITEA

Sarmad Hasan Ahmed Al-Maawi

Electrical Engineer

Nanotechnology Master Student at Ondokuz Mayis University

Education:

Bachelor's degree / Electrical Engineering, University of Technology, Iraq – Baghdad, September 1999

Diploma / Electronics at Electronic Institution, Iraq – Baghdad, October 1994

Languages:

English / Level: Expert

Arabic / Level: Expert

French / Level: Expert

German / Level: Beginner

Turkish / Level: Beginner

Contact Information :

ORCID ID : **0000-0002-9569-9533**

Publications :

1. Sarmad Almaawi, The correlation between the refractive error of patient and the degree of squint, Megger Limited, December 2022.

2. Sarmad Hasan Ahmed AL-MAAWI and Ömer ANDAÇ, Metal-organic Framework Composite-Based Materials for Hybrid Supercapacitor, 2nd International Congress on Multidisciplinary Natural Sciences and Engineering 1-2 Dec 2022, Ankara

Won Awards, Incentives and Scholarships

1.Proper testing of DC High Speed Circuit breakers certificate